

Wintertime aerosol chemistry and haze evolution in an extremely polluted city of North China Plain: significant contribution from coal and biomass combustion

By Haiyan Li et al.

We thank the reviewers for their thoughtful and constructive comments. We have carefully revised the manuscript accordingly. Our point-to-point responses can be found below, with reviewer comments repeated in black and author responses in blue. Changes made to the manuscript are in quotation marks.

Author Responses to Anonymous Referee #1

This paper presents ACSM results from a heavily polluted city in China during wintertime. The PM₁ concentrations averaged at 187.6 ug/m³, in urgent need to elucidate the characteristics of the PM pollution. The paper is overall well written and the figures are informative, I recommend its publication after addressing a few issues listed below.

(1) This reviewer finds that some necessary discussions are lacking in the manuscript. The PM₁ contains a significant fraction of chloride - 9%. This fraction is in fact higher than the chloride level typically observed in other AMS studies. Considering the PM₁ concentration is high, chloride concentration is also significant. I think its sources, formation and other characteristics should be discussed. (2) Similar as the comment 1, characteristics of BC should be discussed in more details as well.

Detailed discussions about chloride and BC have been added in Section 3.1. “The average chloride contribution (9%) is relatively high compared to that previously observed in NCP region. Submicron nonrefractory chloride in the aerosol phase can be directly emitted from different sources (e.g., biomass burning and coal combustion) (Lobert et al., 1999; McCulloch et al., 1999), and formed in the atmosphere through gas-to-particle conversion (e.g., NH₄Cl partitioning) (Baek et al., 2006). Considering that chloride demonstrated pronouncedly enhanced peaks during night and it showed good correlations with CCOA and BBOA ($r=0.72$ and 0.80 , respectively), a large fraction of chloride during wintertime was thought to be from primary emissions at night. On average, BC accounted for 5% of total PM₁. Its distinct peaks at morning and evening rush hours suggested that BC was mainly associated with traffic emissions.”

(3) Introduction: The authors state that regional transport is a major factor for the heavy haze formation in Beijing. Any comments on the role of local new particle formation and growth?

In the introduction, we have added the following information of the importance of new particle formation and growth on haze formation in NCP region: “New particle formation and growth also plays an important role in haze formation. By examining in detail the haze events under typical fall conditions in Beijing, Guo et al. (2014) indicated that nucleation consistently

preceded a polluted period with high number concentrations and the development of the episode involved efficient and sustained growth from the nucleation-mode particles over multiple days.”

(4) The authors sometimes use r and sometime r_2 , it is better to be consistent throughout the manuscript.

We have changed all the r_2 to r to be consistent throughout the manuscript.

(5) The mass fraction of PM_{10} to TEOM-determined $PM_{2.5}$ is about 88%, which appeared to be higher than those values in other studies. This probably can be discussed in more details.

According to the values reported in the literature, the ratio of PM_{10} to TEOM-determined $PM_{2.5}$ mostly varied from 0.67 to 0.77 in NCP region (Sun et al., 2013; Sun et al., 2014; Zhang et al., 2014; Sun et al., 2015; Hu et al., 2016). But a high $PM_{10}/PM_{2.5}$ ratio of 0.90 was also observed by Jiang et al. (2015) during wintertime in Beijing. So the value of 0.88 for $PM_{10}/PM_{2.5}$ in this study appeared to be a bit higher. The difference may be due to: (1) the contribution of semi-volatile species to $PM_{2.5}$ varied greatly among different periods and different locations, because TEOM is heated to 50 °C during the measurement, which might have caused significant losses of semi-volatile species, e.g., ammonium nitrate and semi-volatile organics; and (2) the contribution of particles in the size range of 1-2.5 μm to the total $PM_{2.5}$ might also be different among different pollution episodes and different sites. Detailed discussion has been added in the manuscript: “Compared to the results reported previously in this area (Sun et al., 2013a; Sun et al., 2014; Zhang et al., 2014; Sun et al., 2015; Hu et al., 2016), the ratio of PM_{10} to TEOM-determined $PM_{2.5}$ in this work appeared to be a bit higher. The difference may be due to: (1) the contribution of semi-volatile species to $PM_{2.5}$ varied greatly among different periods and different locations, because TEOM is heated to 50 °C during the measurement, which might have caused significant losses of semi-volatile species, e.g., ammonium nitrate and semi-volatile organics; and (2) the contribution of particles in the size range of 1-2.5 μm to the total $PM_{2.5}$ might also change among different pollution episodes and different sites.”

(6) The PMF-ME2 algorithm didn’t resolve a cooking OA factor. Did the authors try to use any sort of reference COA profile in the PMF analyses, and were any reference BBOA, CCOA profile used as input? (as it was only mentioned HOA profile was used as input).

We only used the HOA reference profile as a constraint of the PMF-ME2 algorithm in this study. As mentioned in Section 2.3, to do OA source apportionment, we attempted to perform PMF analysis with the PMF2 algorithm at first, which requires no a priori information about factor profiles or time trends. But in the PMF solution, the resolved CCOA factor seemed to be mixed with the signals from HOA, especially considering the two noticeable peaks during morning and evening rush hours in the diurnal profile. This is the reason why we decided to redo OA source apportionment with the HOA reference profile as the input of the PMF-ME2 algorithm. For BBOA and CCOA, the model itself could obviously resolve these two factors without any constraint. Because the BBOA and CCOA profile may vary among different

periods and different locations, we prefer not to constrain the model with BBOA and CCOA reference profile obtained from previous studies. For the cooking OA factor, we did not see any obvious signals of this factor in our solution. Therefore, we prefer not to manually force the model to resolve a cooking OA factor. The reason that a cooking OA factor is not resolved in this study is probably due to its minor concentration and contribution to total OA during wintertime in Handan, even lower than HOA.

(7) The weekdays didn't include Monday and the weekends didn't include Saturday. Was this treatment consistent with and were often used in previous studies?

Yes, this treatment was often used in previous studies. Observations indicate that Monday and Saturday behave as intermediate between weekdays and weekends due to significant memory of the previous day's emissions (Murphy et al., 2007). Therefore, many previous studies omit Monday and Saturday to reduce unnecessary bias in the weekday and weekend values, respectively (Russell et al., 2010; Revuelta et al., 2012; Choi et al., 2013; Young et al., 2016).

(8) In Figure 9, this reviewer feels the nitrate fraction increased and then decreased with the increase of PM₁ loading rather than only a general decreasing trend.

We agree with the reviewer that the nitrate fraction increased a bit and then decreased with the increase of PM₁ loading as shown in Figure 9. The corresponding description has been revised: "The nitrate fraction went up a bit and then showed a decreasing trend with increasing PM₁ mass loading whereas the contribution of sulfate increased from 12% to 20% as PM₁ concentration developed from 100 $\mu\text{g}/\text{m}^3$ to 600 $\mu\text{g}/\text{m}^3$."

(9) Figure 11 is for the entire study period, correct? But it was placed in the case study, it probably should be made clear in the figure caption to avoid confusion.

Thanks for the suggestion. Yes, Figure 11 is for the entire study period. We put this figure in the case study to demonstrate the effects of meteorological conditions. We have made it clear in the figure caption to avoid confusion.

(10) in line 170-175, the authors stated that combustion emissions were significant as it had a good correlation with CO, but the traffic HOA in factor is only a minor contributor to the total OA. I understand the combustion does not only refer to traffic combustion emissions. But this probably should be stated clearly.

We have stated this clearly in the manuscript: "Interestingly, the temporal pattern of organics tracked well with that of CO ($r = 0.84$, Fig.2), implying that combustion emissions were a significant source of organic aerosols in Handan, i.e., traffic, coal combustion, and biomass burning."

Author Responses to Anonymous Referee #2

General Comments

This manuscript discusses a wintertime field campaign in the North China Plain during an extreme haze period. The authors evaluate the sources of primary and secondary PM and discuss the evolution of PM constituents and gaseous pollutants in light of prevailing meteorological conditions. The paper is well-written and provides full documentation of the methods, calculations, analyses performed, and conclusions based on these analyses. Given the manuscript's focus on field measurements, the evolution of pollutants within air polluted air masses, and a geographic area that hasn't been the subject of many intensive field campaigns, this manuscript falls within the scope of ACP. I have no major comments on the manuscript, but present a set of minor comments in the "Specific Comments" and "Technical Corrections" sections below. I do note that for future manuscripts, the authors should ensure that every line is numbered, as reviewers of this manuscript had to count lines to ensure that the correct line numbers were cited.

We thank the reviewer for the positive comments. We ensure that every line is numbered for future manuscripts.

Specific Comments

1. Line 44: "may cause climate change" is very vague. This should be expanded to a sentence discussing radiative forcings and the indirect and direct effects of PM.

We have revised the sentence to "Aerosols can reduce visibility, adversely affect human health (Pope and Dockery, 2006), and influence climate change directly by absorbing and reflecting solar radiation and indirectly by modifying cloud formation and properties (Pöschl, 2005; Seinfeld and Pandis, 2012)..."

2. Line 153: The CNAAQs is quite high compared to PM standards in other countries. It would be helpful to compare the CNAAQs here to international standards to give readers a broader picture of the percent of days that had high PM.

Thanks for the suggestion. The US National Ambient Air Quality Standards for 24-h $PM_{2.5}$ was added for comparison. The sentence was revised to "Based on TEOM measurements, only 4 days met the US National Ambient Air Quality Standards (NAAQS, $35 \mu\text{g}/\text{m}^3$ for the 24 h average of $PM_{2.5}$) and 13 days met the Chinese NAAQS Grade II ($75 \mu\text{g}/\text{m}^3$ for the 24 h average of $PM_{2.5}$) for the whole study period of 65 days. In other words, the daily average $PM_{2.5}$ concentrations exceeded the US NAAQS and the Chinese NAAQS on 94% and 80% of the days, respectively (Fig. 2)."

3. Line 155: Explain how "red haze alarms" are calculated.

Because there are some criteria for the red haze alarm, a website was referenced for explanation. The sentence was revised to "On December 22, the daily $PM_{2.5}$ concentration reached the highest value of $725.7 \mu\text{g}/\text{m}^3$, leading to the first "red" haze alarm (http://www.cma.gov.cn/kppd/kppdsytj/201310/t20131028_229921.html) ever in Hebei Province."

4. Figure S9: This figure is a key piece of information related to your argument in lines 170-175. I suggest moving this figure from the supplement to the main document.
The statement in lines 170-175 is related to Figure 2 rather than Figure S9. Figure S9 only presents the diurnal pattern of the mass fractions of aerosol species. Instead of moving Figure S9, we have clearly noted “Fig.2” in the corresponding statement.
5. Line 173: I don’t agree with your definition of "background." It would be more correct to simply state that ozone concentrations were nearly zero during haze episodes, as these episodes cannot be considered background time periods.
The sentence has been revised according to the suggestion of the reviewer.
6. Line 194: Define the acronyms WS and WD here.
Because the acronyms WS and WD have been defined in line 115, we kept these two acronyms in line 194. We have corrected the error in definition “wind direction (WS)” in line 115 to “wind direction (WD)”.
7. Line 195: It’s not clear how figure S10 supports this argument, and this should be clarified.
Bivariate polar plots show how the concentration of a pollutant varies by the wind direction and wind speed at a receptor site. As shown in Figure S10, HOA demonstrated high concentrations under relatively low wind speed (<1.5m/s), suggesting that HOA was largely contributed by local emission sources rather than regional transport. For further clarification, we revised the sentence as “Bivariate polar plots, which present the concentrations of air pollutants as a function of WS and WD using the OpenAir software (Carslaw and Ropkins, 2012), demonstrated higher concentrations of HOA under relatively low WS (<1.5m/s), suggesting that HOA was substantially influenced by local emission sources, in accordance with its primary characteristics (Fig. S10).”
8. Lines 216-218: The final sentence in this paragraph is an opinion, not a result, and therefore should be moved to the conclusions.
We think that for the section “Results and discussions”, not only the results should be included but also some discussions on the results. The last sentence in line 216-218 is a discussion following the high concentration of CCOA in Handan. Therefore, we kept the sentence in this paragraph. In the conclusions, a suggestion of technology-based emission controls on coal combustion for policy makers was also mentioned.
9. Line 385: What evidence do you have that f_N increased? To me, it appears that the median f_N at 90-100% is the same as at 20-40%.
Here, we were discussing the different behavior of f_S and f_N when $RH > 50\%$. Although the increase of f_N is not significant, it showed a small increase at RH 60-70% and then decreased a bit at RH 90-100%. To avoid confusion, we revised the sentence in Line 385 to “ f_N showed a small increase at RH 60-70% and then decreased a bit when $RH > 90\%$ ”.

10. Lines 412-413: Clarify what is meant by "low efficient combustion."

For clarification, we revised the sentence to “This is mainly related to large emissions of air pollutants from coal and biomass combustion during wintertime, especially for simple household stoves with low combustion efficiency.”

Technical Corrections

1. Line 56: "combustions" should be "combustion"

The text has been changed accordingly. Also changed for the title.

2. Line 225: "the" should be inserted between "during" and "biomass"
Inserted.

3. Line 392: "For another" doesn't fit well here. I suggest changing this to "Another explanation is that"

We have reworded accordingly.

4. Line 421: "northeastern" should be changed to "northwestern"
Corrected.

References

Baek, B. H., Koziel, J., and Aneja, V. P.: A preliminary review of gas-to-particle conversion, monitoring, and modeling efforts in the USA. *Int. J. Global Environ. Iss.*, 6 (2/3), 204–230, 2006.

Carlaw, D. C. and Ropkins, K.: openair - An R package for air quality data analysis, *Environmental Modelling & Software*, 27-500 28, 52-61, 2012.

Choi, W., Paulson, S. E., Casmassi, J., and Winer, A. M.: Evaluating meteorological comparability in air quality studies: Classification and regression trees for primary pollutants in California's South Coast Air Basin, *Atmos Environ*, 64, 150-159, 10.1016/j.atmosenv.2012.09.049, 2013.

Guo, S., Hu, M., Zamora, M. L., Peng, J. F., Shang, D. J., Zheng, J., Du, Z. F., Wu, Z., Shao, M., Zeng, L. M., Molina, M. J., and Zhang, R. Y.: Elucidating severe urban haze formation in China, *P Natl Acad Sci USA*, 111, 17373-17378, 10.1073/pnas.1419604111, 2014.

Hu, W., Hu, M., Hu, W., Jimenez, J. L., Yuan, B., Chen, W., Wang, M., Wu, Y., Chen, C., Wang, Z., Peng, J., Zeng, L., and Shao, M.: Chemical composition, sources and aging process of submicron aerosols in Beijing: contrast between summer and winter, *J. Geophys. Res.*, 121, 1955–1977, doi:10.1002/2015JD024020, 2016.

Jiang, Q., Sun, Y. L., Wang, Z., and Yin, Y.: Aerosol composition and sources during the Chinese Spring Festival: fireworks, secondary aerosol, and holiday effects, *Atmos Chem Phys*, 15, 6023-6034, 10.5194/acp-15-6023-2015, 2015.

Lobert, J. M., Keene, W. C., Logan, J. A., and Yevich, R.: Global chlorine emissions from biomass burning: Reactive Chlorine Emissions Inventory, *J Geophys Res-Atmos*, 104, 8373-8389, Doi 10.1029/1998jd100077, 1999.

McCulloch, A., Aucott, M. L., Benkovitz, C. M., Graedel, T. E., Kleiman, G., Midgley, P. M., and Li, Y. F.: Global emissions of hydrogen chloride and chloromethane from coal combustion, incineration and industrial activities: Reactive Chlorine Emissions Inventory, *J Geophys Res-Atmos*, 104, 8391-8403, Doi 10.1029/1999jd900025, 1999.

Murphy, J. G., Day, D. A., Cleary, P. A., Wooldridge, P. J., Millet, D. B., Goldstein, A. H., and Cohen, R. C.: The weekend effect within and downwind of Sacramento - Part 1: Observations of ozone, nitrogen oxides, and VOC reactivity, *Atmos Chem Phys*, 7, 5327-5339, 2007.

Pope III, C. A. and Dockery, D. W.: Health Effects of Fine Particulate Air Pollution: Lines that Connect, *J. Air Waste Manage.* 56, 709–742, 2006.

Pöschl, U.: Atmospheric Aerosols: Composition, Transformation, Climate and Health Effects, *Angew. Chem. Int. Ed.*, 44, 7520–7540, 2005.

Revuelta, M. A., Harrison, R. M., Nunez, L., Gomez-Moreno, F. J., Pujadas, M., and Artinano, B.: Comparison of temporal features of sulphate and nitrate at urban and rural sites in Spain and the UK, *Atmos Environ*, 60, 383-391, 10.1016/j.atmosenv.2012.07.004, 2012.

Russell, A. R., Valin, L. C., Bucsela, E. J., Wenig, M. O., and Cohen, R. C.: Space-based Constraints on Spatial and Temporal Patterns of NO_x Emissions in California, 2005-2008, *Environ Sci Technol*, 44, 3608-3615, 10.1021/es903451j, 2010.

Seinfeld, J. H. and Pandis, S. N.: *Atmospheric Chemistry and Physics: From Air Pollution to Climate Change*, John Wiley & Sons, New York, 2nd edition, 1232 pp., ISBN-13: 978-0-471-72018-8, 2006.

Sun, Y. L., Wang, Z. F., Fu, P. Q., Yang, T., Jiang, Q., Dong, H. B., Li, J., and Jia, J. J.: Aerosol composition, sources and processes during wintertime in Beijing, China, *Atmos. Chem. Phys.*, 13, 4577-4592, doi:10.5194/acp-13-4577-2013, 2013.

Sun, Y., Jiang, Q., Wang, Z., Fu, P., Li, J., Yang, T., and Yin, Y.: Investigation of the Sources and Evolution Processes of Severe Haze Pollution in Beijing in January 2013, *J. Geophys. Res.*, 119, 4380–4398, 2014.

Sun, Y. L., Wang, Z. F., Du, W., Zhang, Q., Wang, Q. Q., Fu, P. Q., Pan, X. L., Li, J., Jayne, J., and Worsnop, D. R.: Long-term real-time measurements of aerosol particle composition in Beijing, China: seasonal variations, meteorological effects, and source analysis, *Atmos. Chem. Phys.*, 15, 10149–10165, doi:10.5194/acp-15-10149-2015, 2015.

Young, D. E., Kim, H., Parworth, C., Zhou, S., Zhang, X. L., Cappa, C. D., Seco, R., Kim, S., and Zhang, Q.: Influences of emission sources and meteorology on aerosol chemistry in a polluted urban environment: results from DISCOVER-AQ California, *Atmos Chem Phys*, 16, 5427-5451, 10.5194/acp-16-5427-2016, 2016.

Zhang, J. K., Sun, Y., Liu, Z. R., Ji, D. S., Hu, B., Liu, Q., and Wang, Y. S.: Characterization of submicron aerosols during a month of serious pollution in Beijing, 2013, *Atmos. Chem. Phys.*, 14, 2887-2903, doi:10.5194/acp-14-2887-2014, 2014.

1 Wintertime aerosol chemistry and haze evolution in an extremely 2 polluted city of North China Plain: significant contribution from coal 3 and biomass combustions

4 Haiyan Li^{1,2}, Qi Zhang², Qiang Zhang^{3,4}, Chunrong Chen³, Litao Wang⁵, Zhe Wei⁵, Shan Zhou², Caroline
5 Parworth², Bo Zheng¹, Francesco Canonaco⁶, André S. H. Prévôt⁶, Ping Chen⁷, Hongliang Zhang⁷,
6 Timothy J. Wallington⁸, Kebin He^{1,4,9}

7 ¹ State Key Joint Laboratory of Environment Simulation and Pollution Control, School of Environment, Tsinghua University,
8 Beijing 100084, China

9 ² Department of Environmental Toxicology, University of California, Davis, CA 95616, USA

10 ³ Ministry of Education Key Laboratory for Earth System Modeling, Center for Earth System Science, Tsinghua University,
11 Beijing 100084, China

12 ⁴ Collaborative Innovation Center for Regional Environmental Quality, Beijing 100084, China

13 ⁵ Department of Environmental Engineering, Hebei University of Engineering, Handan, Hebei 056038, China

14 ⁶ Laboratory of Atmospheric Chemistry, Paul Scherrer Institute, 5232 PSI Villigen, Switzerland

15 ⁷ Handix LLC, Boulder, CO 8031, USA

16 ⁸ Research & Advanced Engineering, Ford Motor Company, Dearborn, Michigan 28121, USA

17 ⁹ State Environmental Protection Key Laboratory of Sources and Control of Air Pollution Complex, Tsinghua University,
18 Beijing 100084, China

19 *Correspondence to:* Qiang Zhang (qiangzhang@tsinghua.edu.cn), Kebin He (hekb@tsinghua.edu.cn)

20 **Abstract.** The North China Plain (NCP) frequently experiences heavy haze pollution, particularly during wintertime. In 2015-
21 2016 winter, the NCP region suffered several extremely severe haze episodes with air pollution red alerts issued in many cities.
22 We have investigated the sources and aerosol evolution processes of the severe pollution episodes in Handan, a typical
23 industrialized city in the NCP region, using real-time measurements from an intensive field campaign during the winter of
24 2015-2016. The average ($\pm 1\sigma$) concentration of submicron aerosol (PM_{1}) during December 3, 2015 – February 5, 2016 was
25 $187.6 (\pm 137.5) \mu\text{g m}^{-3}$, with the hourly maximum reaching $700.8 \mu\text{g m}^{-3}$. Organic was the most abundant component, on
26 average accounting for 45% of total PM_{1} mass, followed by sulfate (15%), nitrate (14%), ammonium (12%), chloride (9%)
27 and BC (5%). Positive matrix factorization (PMF) with multi-linear engine (ME-2) identified four major organic aerosol (OA)
28 sources, including traffic emissions represented by a hydrocarbon-like OA (HOA, 7% of total OA), industrial and residential
29 burning of coal represented by a coal combustion OA (CCOA, 29% of total OA), open and domestic combustion of wood and
30 crop residuals represented by a biomass burning OA (BBOA, 25% of total OA), and formation of secondary OA (SOA) in the
31 atmosphere represented by an oxygenated OA (OOA, 39% of total OA). Emissions of primary OA (POA), which together
32 accounted for 61% of total OA and 27% of PM_{1} , are a major cause of air pollution during the winter. Our analysis further
33 uncovered that, primary emissions from coal combustion and biomass burning together with secondary formation of sulfate
34 (mainly from SO_2 emitted by coal combustion) are important driving factors for haze evolution. However, the bulk composition
35 of PM_{1} showed comparatively small variations between less polluted periods (daily $PM_{2.5} \leq 75 \mu\text{g m}^{-3}$) and severely polluted
36 periods (daily $PM_{2.5} > 75 \mu\text{g m}^{-3}$), indicating relatively synchronous increases of all aerosol species during haze formation.

37 The case study of a severe haze episode, which lasted 8 days starting with a steady build-up of aerosol pollution followed by
38 a persistently high level of PM₁ (326.7 – 700.8 µg m⁻³), revealed the significant influence of stagnant meteorological conditions
39 which exacerbate air pollution in the Handan region. The haze episode ended with a shift of wind which brought in cleaner air
40 masses from the northwest of Handan and gradually reduced PM₁ concentration to < 50 µg m⁻³ after 12 hours. Aqueous-phase
41 reactions under higher relative humidity (RH) were found to significantly promote the production of secondary inorganic
42 species (especially sulfate), but showed little influence on SOA.

43 1 Introduction

44 Atmospheric particles are a complex mixture of species emitted directly to the atmosphere or formed via gas-to-particle
45 conversions. Aerosols ~~can reduce visibility, have adverse effects on~~ adversely affect human health (Pope and Dockery, 2006),
46 and ~~may cause~~ influence climate change directly by absorbing and reflecting solar radiation and indirectly by modifying cloud
47 formation and properties (Pöschl, 2005; Seinfeld and Pandis, 2012), all of which are intrinsically linked to the chemical
48 composition of aerosols. Therefore, it is crucial to gain a quantitative understanding of aerosol composition and evolution
49 processes for accurately assessing the environmental effects of aerosols.

50 With the rapid economy growth and urbanization in North China Plain (NCP), air pollution in this region has become a
51 severe problem and a source of concern. Hebei Province, located in the NCP region, is known for persistent air quality problems
52 and extreme haze pollution events. According to the Ministry of Environmental Protection (MEP) of China, 7 out of the top
53 10 polluted cities in China in 2015 were located in Hebei province. During the extremely severe haze event that occurred in
54 the winter of 2015-2016 in the NCP region, the hourly peak PM_{2.5} concentration in southern Hebei exceeded 1000 µg/m³. It is
55 well known that the severe air pollution in the NCP region was caused by large anthropogenic emissions and unfavorable
56 meteorological conditions. Emissions of primary PM_{2.5}, sulfur dioxide (SO₂), and nitrogen oxides (NO_x) from Hebei in 2015
57 are estimated to account for 8 %, 6 %, and 7 % of China's national total emissions respectively (<http://meicmodel.org/>), with
58 large contributions from coal and biomass combustions.

59 Large anthropogenic emissions in the NCP region have degraded regional air quality significantly. Extensive studies have
60 been conducted to explore the sources and evolution of haze episodes in Beijing, especially with the wide application of
61 Aerodyne Aerosol Mass Spectrometer (AMS)/Aerosol Chemical Speciation Monitor (ACSM) for online measurement of
62 aerosol chemical composition (Takegawa et al., 2009; Sun et al., 2010; Sun et al., 2012, 2013a, 2013b, 2014, 2015, 2016a,
63 2016b; Zhang et al., 2014; Hu et al., 2016). These studies have noted that regional air transport from the south or east
64 surrounding regions, unfavorable synoptic conditions, and heterogeneous secondary reactions associated with high RH
65 initiated the rapid formation and persistent evolution of haze episodes in Beijing. During a record-breaking haze episode in
66 wintertime in Beijing, Sun et al. (2014) estimated that regional transport contributed up to 66% to the steep rise of air pollutants
67 in Beijing. New particle formation and growth also plays an important role in haze formation. By examining in detail the haze
68 events under typical fall conditions in Beijing, Guo et al. (2014) indicated that nucleation consistently preceded a polluted

69 period with high number concentrations and the development of the episode involved efficient and sustained growth from the
70 nucleation-mode particles over multiple days. In addition, organic aerosol (OA) was found to be a major component of aerosol
71 particles, accounting for more than one-third of total PM₁ mass. The primary OA (POA) from traffic, cooking, biomass burning,
72 coal combustion, etc., and secondary OA (SOA) have been distinguished and quantified mainly using positive matrix
73 factorization (PMF; Paatero and Tapper, 1994). Recently, a novel PMF procedure, with the multi-linear engine (ME-2)
74 algorithm, was developed to apportion the OA sources in Beijing and Xi'an, allowing for a more objective selection of source
75 apportionment solution (Elser et al., 2016). However, our knowledge of the sources and aerosol evolution processes for the
76 whole region still remains incomplete and is especially limited for areas outside of Beijing. For other cities in the NCP region,
77 such as Hebei province, only a limited number of aerosol studies have been conducted using offline filter-based measurement
78 techniques (Zhao et al., 2013; Wei et al., 2014). Due to low time resolution varying from one day to several days, these studies
79 provided relatively limited information on aerosol emission sources and formation processes, thus it remains unclear how the
80 rapid haze evolution happens and what the driving sources are for the air pollution problems in Hebei. Therefore, it is crucial
81 to conduct research in the areas outside of Beijing, especially many provinces subjected to high anthropogenic emissions,
82 which may provide critical information to help air pollution policy making to be more direct and efficient.

83 To fill this knowledge gap, an intensive field campaign with multiple state-of-the-art research instruments was conducted
84 in Handan, a major city in southern Hebei, during the winter of 2015-2016. Handan is located in the intersectional area of four
85 provinces, Hebei, Shanxi, Henan and Shandong, all of which are heavily urbanized and industrialized (Fig. 1a). Handan itself
86 is also well known for heavy industrial production of steel, iron and cement, which result in high local emissions of air
87 pollutants. According to the routine monitoring of the China National Environmental Monitoring Center (CNEMC) from 2013
88 to 2015, Handan is always listed as one of the top 10 polluted cities in China. Hence, this location and its specific conditions
89 allow for a detailed exploration of aerosol chemistry and haze evolution processes under high anthropogenic emissions.

90 Here, we provide both overview and evolution cycle analyses of aerosol characteristics using aerosol data acquired with
91 an ACSM and collocated measurements of black carbon (BC), meteorological conditions and gas phase species. The sources
92 of OA are investigated in detail using PMF solved with the ME-2 algorithm (Paatero, 1999). Comparison of species diurnal
93 cycles between weekdays and weekends, polluted and non-polluted days, and the variation of aerosol characteristics with
94 increasing PM₁ concentration, provide insights into the driving factors for haze evolution. We also examine the impacts of
95 meteorological conditions based on an intense evolution case of submicron aerosol.

96 **2 Experimental methods**

97 **2.1 Sampling site and instrumentation**

98 In situ measurements were conducted at Hebei University of Engineering (36.57° N, 114.50° E) in Handan from
99 December 3, 2015 to February 5, 2016. Our sampling site is situated in the southeast edge of urban Handan, on the roof of a

100 four-story building (~12 m high), surrounded by the school and residential area, ~300 m north of the South Ring Road, and
101 ~400 m northeast of Handa Highway (S313). The ambient temperature varied from -12.7 to 14.4 °C, with an average of 1.8
102 °C. The prevailing wind came from the northeast and southwest, characterized by low wind speeds (Fig. 1b).

103 The mass concentrations of non-refractory submicron aerosol (NR-PM₁), including organics, sulfate, nitrate, ammonium,
104 and chloride, were measured in situ using an Aerodyne ACSM. The detailed description of this instrument can be found in Ng
105 et al. (2011a). In brief, ambient air was sampled through a PM_{2.5} cyclone to remove coarse particles with diameters exceeding
106 2.5 μm and then traversed a 2-m-long, ½-inch (outer diameter) stainless steel tube at a flow rate of 3 L min⁻¹ using an external
107 pump. A Nafion dryer was installed before the ACSM to dry aerosol samples and maintain the RH below 30%. Subsequently,
108 only a subset of the flow at ~85 cc min⁻¹ was sampled through a 100 μm critical orifice, focusing aerosol particles between 40
109 nm and 1 μm into the vacuum chamber via an aerodynamic lens. In our study, the ACSM mass spectrometer was operated at
110 a scanning speed of 200 ms per amu from 10 to 150 amu. By automatically switching 14 cycles between filter mode and
111 sample mode, the time resolution for the ACSM data in this study was approximately 15 minutes.

112 Because of the limit of the vaporizer temperature (~600 °C), the ACSM could not measure refractory species such as BC.
113 Thus a multi-angle absorption photometer (MAAP, Thermo Scientific model 5012) was deployed for real-time measurement
114 of BC concentration. The MAAP was operated at an incident light wavelength of 670 nm, with a PM₁ cyclone and a drying
115 system incorporated in front of the sampling line (Petzold and Schönlinner, 2004; Petzold et al., 2005). Online PM_{2.5} mass
116 concentration was measured simultaneously using a heated Tapered Element Oscillating Microbalance (TEOM series 1400a,
117 Thermo Scientific). Other collocated instruments included a suite of commercial gas analyzers (Thermo Scientific) to monitor
118 the variations of gaseous species (i.e., CO, O₃, NO, NO₂, NO_x, and SO₂). Meteorological parameters, i.e. temperature, RH,
119 pressure, wind speed (WS) and wind direction (WDS), were obtained by a Lufft WS500-UMB Smart Weather Sensor. The
120 data reported in this paper are in Beijing Time (BJT: UTC+8).

121 2.2 ACSM Data analysis

122 The mass concentrations of non-refractory aerosol species and the spectral matrices of OA were processed using ACSM
123 standard data analysis software (v 1.5.3.5) within Igor Pro version 6.37. The detailed procedures have been described in Ng et
124 al. (2011a). The default relative ionization efficiency (RIE) values were used for organics (1.4), sulfate (1.19), nitrate (1.1),
125 and chloride (1.3), whereas the RIE of ammonium (6.28) was directly determined via analyzing pure NH₄NO₃ particles. To
126 account for the incomplete detection of aerosol species, a default collection efficiency (CE) value of 0.5 was applied to the
127 entire data set as aerosol particles were dried before ACSM sampling and the ammonium nitrate fraction was always lower
128 than 0.4 during the whole period. Although previous studies have shown that aerosol particles may be slightly acidic during
129 wintertime in the NCP region, particle acidity was not high enough to affect CE values substantially (Sun et al., 2016a). As
130 shown in Fig. S1 in the supplementary information, the mass concentrations of PM₁ (= NR-PM₁ + BC) correlated tightly with
131 total PM_{2.5} mass loadings measured by TEOM (slope=0.88, r²=0.9387). Compared to the results reported previously in this
132 area (Sun et al., 2013a; Sun et al., 2014; Zhang et al., 2014; Sun et al., 2015; Hu et al., 2016), the ratio of PM₁ to TEOM-

133 determined PM_{2.5} in this work appeared to be a bit higher. The difference may be due to: (1) the contribution of semi-volatile
134 species to PM_{2.5} varied greatly among different periods and different locations, because TEOM is heated to 50 °C during the
135 measurement, which might have caused significant losses of semi-volatile species, e.g., ammonium nitrate and semi-volatile
136 organics; and (2) the contribution of particles in the size range of 1-2.5 μm to the total PM_{2.5} might also change among different
137 pollution episodes and different sites.

138 **2.3 Positive Matrix Factorization of organic aerosol matrix**

139 To determine potential sources of OA, the ACSM mass spectra were processed using the ME-2 algorithm implemented
140 with the toolkit SoFi (Source Finder) developed by Canonaco et al. (2013). The so-called *a* value approach allows the user to
141 introduce a priori information in forms of known factor profiles or time series to obtain a rather unique solution and thus reduce
142 the rotational ambiguity of the PMF2 algorithm. The spectra and error matrices of organics were prepared according to the
143 protocol summarized by Ulbrich et al. (2009) and Zhang et al. (2011). Given the interferences of the internal standard of
144 naphthalene at *m/z* 127-129 and the low signal-to-noise ratio of larger ions, we only considered ions up to *m/z* 120 in this study.
145 A reference HOA profile, which is an average of multiple ambient data sets taken from Ng et al. (2011b), was introduced to
146 constrain the model performance with *a* value varying from 0 to 1. Following the guidelines presented by Canonaco et al.
147 (2013) and Crippa et al. (2014), an optimal solution involving four factors with *a* value of 0.1 was accepted. Detailed analyses
148 of the factor time series, mass spectra, diurnal patterns, and correlations with external tracers can be found in the supplementary
149 information (Fig. S2-S6). Note that before using the ME-2 engine, we also attempted to perform PMF analysis with the PMF2
150 algorithm for 1 to 8 factors. The solutions were thoroughly evaluated following the recommendations outlined in Zhang et al.
151 (2011) and the results of three- and four-factor solutions at $f_{\text{peak}}=0$ are shown in Fig. S7-S8. The three-factor solution indicates
152 the identification of a coal combustion OA (CCOA), a biomass burning OA (BBOA) and an oxygenated OA (OOA). But the
153 CCOA factor seems to be mixed with the signals from hydrocarbon-like components related to traffic emissions, which is
154 especially evident given the two noticeable peaks in the diurnal profile of the CCOA-factor during morning and evening rush
155 hours. In the four-factor solution, the additional factor could not be physically explained and showed indications of factor
156 splitting. Solutions with 5 to 8 factors show further splitting and mixing of factors. Our inability to separate an individual HOA
157 factor using the PMF2 algorithm is probably due to the minor contribution of traffic emissions in Handan, consistent with the
158 fact that the PMF2 algorithm tends to have difficulty in accurately retrieving minor factors (Ulbrich et al., 2009).

159 **3 Results and discussions**

160 **3.1 Overview of aerosol characteristics**

161 Frequent and persistent haze episodes were observed during the campaign, especially from December 16 to December
162 25, 2015, when an extremely polluted and long-lasting haze event occurred. Based on TEOM measurements, only ~~413~~ 413 days
163 met the US National Ambient Air Quality Standards (NAAQS, 35 μg/m³ for the 24 h average of PM_{2.5}) and 13 days met the

164 Chinese ~~National Ambient Air Quality Standard~~ NAAQS Grade II (~~CNAAQS~~, 75 $\mu\text{g}/\text{m}^3$ for the 24 h average of $\text{PM}_{2.5}$) for the
165 whole study period of 65 days. In other words, the daily average $\text{PM}_{2.5}$ concentrations exceeded the US NAAQS and the
166 Chinese NAAQS on 94% and 80% of the days, respectively (Fig. 2). On December 22, the daily $\text{PM}_{2.5}$ concentration reached
167 the highest value of 725.7 $\mu\text{g}/\text{m}^3$, leading to the first “red” haze alarm
168 (http://www.cma.gov.cn/kppd/kppdsytj/201310/t20131028_229921.html) ever in Hebei Province. The meteorological
169 conditions were stagnant with calm winds throughout the study period (WS usually less than 1.5 m/s), although relatively high
170 WS (generally > 1.5 m/s) with cleaner air from northwest of Handan occasionally interrupted the haze evolution process (Fig.
171 2b). The RH varied from 11.7% to 94.8%, generally with higher values for more polluted periods and lower values during
172 cleaner periods. No precipitation occurred throughout the entire campaign.

173 Hourly PM_{10} concentrations fluctuated dramatically from 4.2 $\mu\text{g}/\text{m}^3$ to 700.8 $\mu\text{g}/\text{m}^3$ (Fig. 2g). The average PM_{10}
174 concentration was 187.6 $\mu\text{g}/\text{m}^3$, more than twice as high as that observed in the well-known severe haze event that occurred in
175 Beijing in January 2013 (Sun et al., 2014; Zhang et al., 2014). Organics constituted a major fraction of PM_{10} , contributing 45%
176 on average during this study, followed by sulfate (15%), nitrate (14%), and ~~ammonium (12%), chloride (9%) and BC (5%)~~.
177 The large fraction of organics in PM_{10} was similar/comparable to previous observations ~~reported~~ in other areas of NCP during
178 wintertime (Sun et al., 2013a; Zhang et al., 2013; Huang et al., 2014). The average chloride contribution (9%) is relatively
179 high compared to that previously observed in NCP region. Submicron nonrefractory chloride in the aerosol phase can be
180 directly emitted from different sources (e.g., biomass burning and coal combustion) (Lobert et al., 1999; McCulloch et al.,
181 1999), and formed in the atmosphere through gas-to-particle conversion (e.g., NH_4Cl partitioning) (Baek et al., 2006).
182 Considering that chloride demonstrated pronouncedly enhanced peaks during night and it showed good correlations with
183 CCOA and BBOA ($r=0.72$ and 0.80 , respectively), a large fraction of chloride during wintertime was thought to be from
184 primary emissions at night. On average, BC accounted for 5% of total PM_{10} . Its distinct peaks at morning and evening rush
185 hours suggested that BC was mainly associated with traffic emissions. In the daytime, PM_{10} was dominated by secondary
186 species because of active photochemistry, whereas the contributions of primary species were significantly increased at night,
187 probably caused by enhanced primary emissions from fuel combustion coupled with shallow boundary layer height (Fig. S9).
188 Ambient CO is an indicator for the intensities of anthropogenic emissions. The hourly CO concentration was as high as
189 10 ppm during the study period, higher than those observed in other areas of China (Andreae et al., 2008; Quan et al., 2014;
190 Yang et al., 2015). Interestingly, the temporal pattern of organics tracked well with that of CO ($r = 0.84$, Fig.2), implying that
191 combustion emissions were a significant source of organic aerosols in Handan, i.e., traffic, coal combustion, and biomass
192 burning. In addition, during severe haze episodes with high NO_x and CO concentrations, ozone remained at the background
193 concentration of almost/nearly zero for several days instead of showing a regular diurnal variation, indicating active ozone
194 titration by NO and a strong influence of primary emissions on haze pollution in this study.

195 3.2 Source apportionment of organic aerosol

196 In this study, three POA factors (HOA, BBOA and CCOA) and one SOA factor (OOA) were resolved by analyzing the

197 ACSM OA mass spectra using the ME-2 algorithm. OOA was the largest contributor to OA mass with an average fraction of
198 39% (Fig. 3). The traffic-related HOA only accounted for 7% of total OA, which was in accordance with the fact that PMF
199 analysis performed with the PMF2 algorithm had difficulty to retrieve it (see Sect. 2.3 for more details). On average, primary
200 sources dominated the OA mass (61%) during this winter study, consistent with the results from previous winter studies in the
201 NCP region (Sun et al., 2013a; Zhang et al., 2014; Hu et al., 2016; Sun et al., 2016a). The discussion below focuses on the
202 characteristics, sources and processes of each OA factor.

203 3.2.1 Hydrocarbon-like OA

204 The HOA factor shows a mass spectrum highly similar to those of freshly emitted traffic or other fossil combustion
205 aerosols (Zhang et al., 2005a; Lanz et al., 2007; Li et al., 2016a). Its profile is dominated by alkyl fragment signatures, the
206 $C_nH_{2n+1}^+$ (m/z 29, 43, 57) and $C_nH_{2n-1}^+$ (m/z 27, 41, 55) ion series. The time series of HOA correlated well with those of NO_x
207 and BC ($r = 0.75$ and 0.74 , respectively, Fig. 3e), two tracers of vehicle emissions. The diurnal pattern of HOA (Fig. 3i) further
208 confirmed the association of HOA with traffic activities, as it showed two obvious peaks during morning and evening rush
209 hours. On average, HOA only accounted for 7% of total OA in Handan; a much smaller fraction than observed in the nearby
210 megacities of Beijing and Tianjin (Sun et al., 2013a; Wang et al., 2015). The small HOA fraction in this study is consistent
211 with findings from a previous source apportionment study which revealed that transportation was a minor source of
212 atmospheric particles in Handan (Wang et al., 2014). Bivariate polar plots, which present the concentrations of air pollutants
213 as a function of WS and WD using the OpenAir software (Carslaw and Ropkins, 2012), demonstrated higher concentrations
214 of HOA under relatively low WS (<1.5m/s), suggesting~~indicated~~ that HOA was substantially-mainly influenced by local
215 emissions sources, in accordance with its primary characteristics (Fig. S10).

216 3.2.2 Coal combustion OA

217 Although coal combustion has rarely been reported as an important source of organic aerosols in the US or Europe, it is
218 a large emitter of organics in China (Cao et al., 2006). According to Zhang et al. (2008b), organic carbon can contribute up to
219 70% of emitted $PM_{2.5}$ for different types of coal combustion in China. During wintertime, coal is the primary fuel for various
220 industries (e.g. power generation, steel milling, and cement production) as well as residential heating in the NCP region. Thus
221 a considerable contribution from coal combustion to OA concentration was expected in this study. Compared to HOA and
222 BBOA, the mass spectrum of CCOA showed strong signals at higher m/z , especially a significant peak at m/z 115, and the
223 temporal trend of CCOA correlated tightly with that of m/z 115 ($r=0.99$, Fig. 3). These findings are similar to observations
224 made in Beijing, Changdao, Xi'an, and Lanzhou during winter, where OA factors representing coal combustion were
225 determined (Hu et al., 2013; Elser et al., 2016; Sun et al., 2016a; Xu et al., 2016). Further, a recent study by Zhou et al. (2016)
226 has shown that the ACSM mass spectra of OA from residential coal combustion emissions tend to present a high peak at m/z
227 115. In addition, CCOA was also found to correlate relatively well with chloride ($r = 0.72$) during this study, consistent with
228 the fact that coal combustion is also an important emission source of chloride.

229 Figure 4 compares the OA composition in this study with those of previous winter studies in China. During wintertime,
230 CCOA was observed to contribute a significant fraction of the fine PM mass in regions to the north of the Yangtze River (e.g.
231 Beijing, Lanzhou, and Handan), due to domestic coal combustion for heating in winter. However, little to no CCOA was
232 observed in areas located to the south of the Yangtze River, e.g. Nanjing, Jiaxing, and Ziyang, mainly reflecting the lack of
233 central heating provided by the Chinese government in this region during winter. In this study, similar to the results observed
234 in Beijing and Lanzhou (Sun et al., 2013a; Hu et al., 2016; Xu et al., 2016), CCOA on average accounted for 29% of total OA,
235 with a minimum of 13% at noon and a maximum of 32% at midnight. However, the average mass concentration of CCOA in
236 Handan ($23.1 \mu\text{g}/\text{m}^3$) was much higher than those observed in previous studies. Given the high consumption of coal and the
237 important role of coal combustion for aerosol pollution in Handan, control of air pollutant emissions from coal combustion
238 through technology renewal is essential for air quality improvement in this area.

239 3.2.3 Biomass burning OA

240 Biomass burning, including wildfires, forest and agricultural burning, and domestic biofuel combustion, is one of the
241 largest emission sources of organics worldwide (Ramanathan et al., 2001). Biomass burning releases air pollutants that have
242 adverse effects on respiratory organs and reduce lung function of human beings (Regalado et al., 2006). In the NCP region,
243 during the harvest seasons in summer and autumn with open agricultural burning, biomass burning is a major influence on
244 aerosol loadings and characteristics. For example, at a suburban site near Beijing during summertime, Sun et al. (2016b)
245 observed that the contribution of BBOA to OA increased from 6% during the non-biomass burning period to 21% during the
246 biomass burning period. During wintertime, as most previous studies of this region were performed in the megacity of Beijing
247 where coal combustion dominates the energy consumption, BBOA was seldom resolved or found to be a minor fraction of
248 total OA mass (Sun et al., 2013a; Zhang et al., 2014; Huang et al., 2014; Sun et al., 2016a). However, for many small and
249 medium-sized cities in the NCP region, domestic combustion of wood and crop residuals for cooking and home heating is very
250 popular in the countryside during wintertime and could emit large amounts of air pollutants (Zhang et al., 2008a; Ding et al.,
251 2012). In Hebei province, biomass burning accounted for 52% of primary organic carbon emissions during the winter of 2015
252 according to the Multi-resolution Emission Inventory for China (MEIC; <http://meicmodel.org/>).

253 In this study, a BBOA factor with high mass concentrations was clearly observed, the mass spectrum of which was
254 characterized by the prominent peaks at m/z 60 and 73, two indicative tracers of biomass burning (Alfarra et al., 2007; Aiken
255 et al., 2009; Lee et al., 2010). The time series of the BBOA varied dramatically and correlated well with that of CO ($r = 0.72$),
256 which was mainly emitted from combustion-related sources. BBOA showed clear diurnal variations with low mass
257 concentrations occurring during daytime and high mass concentrations arising at night. Consistent with the emission inventory,
258 BBOA on average accounted for 25% of total OA mass, with an average concentration of $20.7 \mu\text{g}/\text{m}^3$, much higher than that
259 observed in other areas of China during wintertime (Fig. 4), indicating the important role of biomass burning emissions in
260 aerosol pollution in Handan. Polar plots showed that high BBOA concentrations were mainly related to local emissions (Fig.
261 S10), probably associated with cooking and residential heating using biofuel.

262 3.2.4 Oxygenated OA

263 Although two or more OOA factors with different oxidation degree and formation pathways have been resolved in
264 previous wintertime studies in China (Xu et al., 2015; Sun et al., 2016a), only one OOA factor was observed in our study. The
265 mass spectrum of OOA presented a pattern similar to those reported before (e.g., Zhang et al., 2005b; Ng et al., 2011c) with a
266 prominent peak at m/z 44 (15.8% of the total OOA signal). In addition, OOA showed a temporal trend similar to those of
267 sulfate and nitrate, and correlated strongly with the sum of secondary inorganic species (SIA = sulfate + nitrate + ammonium)
268 (Fig. 5). The polar plots of OOA and secondary inorganic species exhibited similar spatial distributions, with high concentration
269 hotspots located in the northeast, especially during polluted periods (Fig. S10). The temporal variation profile of OOA was
270 much different from those of the POA factors ($r^2 = 0.5025$; Fig. 5). As shown in Fig. 3, while POA varied dramatically between
271 day and night due to the influence of local emissions, the mass concentrations of OOA often built up gradually and remained
272 at high levels for several days until being swept away by clean air masses. These results are consistent with OOA being
273 representative of SOA. Although the diurnal profile of OOA was overall flat in this study, the mass fraction of OOA to total
274 OA increased significantly during daytime, reaching a maximum of 64% at 14:00 BJT (Fig. 3n).

275 3.3 Diurnal variations and insights into aerosol sources

276 3.3.1 Weekdays versus weekends

277 As air pollutants are mainly emitted from anthropogenic sources in Handan, comparing the diurnal profiles of aerosol
278 species between weekdays and weekends would provide insights into the variations of different emission sources and
279 atmospheric processes. Generally speaking, weekdays span Monday to Friday, whereas weekends include Saturday and Sunday.
280 However, because the physical and chemical processes in the atmosphere are not completed instantaneously, the variations of
281 aerosol species may be influenced by the carry-over effect of the previous day. Thus, we alternatively define weekdays from
282 Tuesday to Friday, and weekends only including Sunday. With this classification, differences in the diurnal variations between
283 weekdays and weekends are more visible. Comparisons of the diurnal cycles using the Monday-Friday and Saturday-Sunday
284 definitions are presented in the supplementary information (Fig. S11).

285 As displayed in Fig. 6, the diurnal variations of meteorological parameters did not significantly change from weekdays
286 to weekends, providing a good opportunity to investigate the influence of anthropogenic activities. As expected, the diurnal
287 pattern of HOA, which is associated with traffic emissions, presented a more distinct morning peak on weekdays. This was
288 also the case for BC, CO, and NO_x, which are all fossil fuel combustion tracers. However, the evening rush hour peaks of these
289 species did not show much of a difference between weekdays and weekends, indicating that human activities in the evening
290 were not significantly reduced on weekends. Other aerosol species showed generally similar diurnal trends for weekdays and
291 weekends, similar to the results observed in Beijing (Sun et al., 2013a). In contrast, stronger weekday vs. weekend differences
292 were observed in the US, where the mass concentrations of aerosol species are obviously lower during weekends (Young et
293 al., 2016; Zhou et al., 2016). Results from the present study reveal that active anthropogenic emissions tend to persist

294 throughout the entire week in polluted regions in Handan, leading to limited differences in the concentrations and compositions
295 of major air pollutants between weekdays and weekends. The exception is traffic emissions, for which the morning rush hour
296 peak is more prominent during weekdays.

297 **3.3.2 Polluted versus non-polluted periods**

298 To gain further insights into the evolution of aerosol particles throughout the day, especially during hazy conditions, we
299 explored the diurnal differences of meteorological conditions and air pollutants between polluted and non-polluted days (Fig.
300 7). According to the CNAAQs Grade II of daily $PM_{2.5}$ concentrations ($75 \mu\text{g}/\text{m}^3$), only the 13 days (out of a total of 65 days)
301 were found to meet the requirement and are considered to be non-polluted in this study; the rest are defined as polluted periods.
302 Note that of these 13 non-polluted days, only 3 days achieved the 24 h CNAAQs Grade I level of $PM_{2.5}$ ($35 \mu\text{g}/\text{m}^3$).

303 The temperature was relatively low throughout the period, averaging 2.1°C and 0.2°C on polluted and non-polluted days,
304 respectively. The RH during polluted periods was slightly higher during daytime, favoring the aqueous-phase processing of
305 atmospheric pollutants. The influence of RH is discussed in detail in Sect. 3.5. Stagnant weather conditions with lower wind
306 speeds were observed on polluted days, especially during nighttime, which would aggravate the accumulation of aerosol
307 pollution. Unsurprisingly, the mass concentrations of aerosol components and the mixing ratios of gaseous species were much
308 higher on polluted days. But the diurnal differences between polluted and non-polluted periods could provide some information
309 regarding their evolutionary processes. The diurnal profiles of secondary inorganic species (i.e. sulfate, nitrate, and
310 ammonium), were flatter on polluted days. For example, in the diurnal profile of nitrate during polluted periods, the maximum
311 and minimum concentrations were different by only 13 % or $4.4 \mu\text{g}/\text{m}^3$. This behavior is consistent with the comparison of
312 polar plots between polluted and non-polluted days, which indicated a significant effect of regional transport on polluted
313 periods for secondary species. In contrast, the diurnal trends of primary aerosol species, e.g. HOA, BBOA, and CCOA, during
314 polluted periods differed substantially from those during non-polluted periods. Compared to the relatively flat diurnal profiles
315 on non-polluted days, the mass concentrations of HOA, BBOA, and CCOA were strongly enhanced at nighttime on polluted
316 days. This suggests that the sharp increases of primary species at night, especially those of BBOA and CCOA, may play an
317 important role in haze formation.

318 **3.4 Evolution of aerosol characteristics with increasing PM_{10} concentration**

319 Identifying the responsible emission sources and formation pathways during haze events is essential to effectively
320 implement emission controls, especially with the increased frequency of haze events during winter. In this study, the whole
321 period is divided into polluted and non-polluted days, as described in Sect. 3.3.2. The average PM_{10} concentration during
322 polluted days ($211 \mu\text{g}/\text{m}^3$) was more than three times higher than that during non-polluted days ($49 \mu\text{g}/\text{m}^3$). However, the
323 average aerosol composition did not show obvious changes between these two types of days, indicating the synchronous
324 increase of all aerosol species (Fig. 8a). Indeed, during polluted days, the average mass concentrations of all aerosol species,
325 except for BC, were approximately four times as high as those during non-polluted days (Fig. 8b). Sulfate, CCOA, and BBOA

326 showed the highest polluted/non-polluted ratios, which were 5.3, 5.0, and 5.5, respectively (Fig. 8b). Given the higher average
327 RH on polluted days (average $\pm 1\sigma = 56.5\pm 18.8\%$) compared to non-polluted days (average $\pm 1\sigma = 40.9\pm 18.7\%$), aqueous-phase
328 processing likely has increased the production of sulfate (Wang et al., 2012; Zheng et al., 2015; Elser et al., 2016). During
329 polluted days, the average oxidation ratio of sulfur (molar ratio of sulfate to sum of sulfate and SO₂) was 0.27, higher than that
330 on non-polluted days (0.16). On the other hand, the strong increases of CCOA and BBOA were possibly caused by enhanced
331 gas-to-particle partitioning associated with high PM mass loadings during polluted periods (Mader et al., 2002). Interestingly,
332 compared to aerosol species, CO showed a lower polluted/non-polluted ratio of approximately 2. A possible reason is that CO
333 has a longer atmospheric lifetime compared to aerosol particles, thus it has a more elevated regional background concentration.
334 Note that the polluted/non-polluted ratios for SO₂ and NO_x were also lower compared to the aerosol species. This is potentially
335 a result of enhanced aqueous phase oxidation of SO₂ and NO_x as well as more efficient wet deposition, since the more polluted
336 periods were generally more humid.

337 Figure 9 further displays the average hourly variations of the mass fractions of aerosol species as a function of PM₁
338 concentration. ~~Similar to the results observed in Beijing during wintertime, the nitrate fraction in PM₁ showed a decreasing~~
339 ~~trend with increasing PM₁ mass loading. The nitrate fraction went up a bit and then showed a decreasing trend with increasing~~
340 ~~PM₁ mass loading~~ whereas the contribution of sulfate increased from 12% to 20% as PM₁ concentration ~~increased-developed~~
341 from 100 $\mu\text{g}/\text{m}^3$ to 600 $\mu\text{g}/\text{m}^3$. Since it was unlikely that the emission sources of the main gaseous precursors of these two
342 species (i.e., NO_x and SO₂) had changed significantly during our study, the observed changes in aerosol compositions suggest
343 different formation mechanisms of nitrate and sulfate during wintertime. The substantially elevated production of sulfate
344 during high PM episodes was likely attributable to higher ambient RH, which facilitated sulfate production through aqueous-
345 phase reactions of SO₂ (Kim et al., 2016; Li et al., 2016b; Sun et al., 2013b). The oxidation ratio of sulfur increased from 0.1
346 to 0.4 when PM₁ concentration raised from $\sim 10 \mu\text{g}/\text{m}^3$ to 600 $\mu\text{g}/\text{m}^3$. The mass fractions of different OA factors varied widely
347 as PM₁ concentrations increased. The contribution of HOA to total PM₁ was minor and remained relatively stable across all
348 mass loadings. However, the mass fractions of CCOA and BBOA increased nearly linearly with PM₁ concentrations rising
349 from $\sim 20 \mu\text{g}/\text{m}^3$ to 300 $\mu\text{g}/\text{m}^3$ and plateaued at higher aerosol loadings. OOA, a surrogate of SOA, showed the opposite PM-
350 loading dependency, and its contribution decreased slightly with increasing PM₁ concentration. The study of Sun et al. (2013a)
351 in Beijing also found a growing contribution of CCOA and a declining contribution of OOA with increasing PM₁
352 concentrations during wintertime. These results reveal the important role of POA in the development of high PM pollution
353 during wintertime. Indeed, the scatter plot of OA vs. PM₁ concentrations (Fig. 9c) demonstrates that higher mass fractions of
354 organics in PM₁ were associated with elevated POA contributions to total OA, especially when PM₁ concentrations were more
355 than 200 $\mu\text{g}/\text{m}^3$ (Fig. 9c). Overall, the results here suggest that secondary formation of sulfate (mainly from SO₂ emitted by
356 coal combustion), and primary emissions of organics from coal combustion and biomass burning are important factors driving
357 the development of winter haze pollution in Handan.

358 3.5 A case study on an intense haze episode and the influence of meteorological conditions

359 From December 14 to December 28, 2015, an extremely severe haze episode occurred and was characterized with a steady
360 build-up of air pollutants, including fine particles and CO, over a period of ~ 5 days (Dec. 17 -21, 2015) followed by
361 approximately 4 days of heavy air pollution, during which the average CO mixing ratio was 6.7 ppm and the average PM₁
362 concentration was 500.1 µg/m³ (Fig. 10). This episode ended on Dec. 25, during which winds from the northwest brought in
363 cleaner air, leading to dramatic reductions of air pollutants. This type of evolutionary process has been frequently observed in
364 Beijing during autumn and winter, and is called “sawtooth cycles” by Jia et al. (2008). In this study, the whole haze cycle was
365 divided into five stages: (1) a clean period (Stage 1), (2) an almost linear increasing period of PM₁ concentration (Stage 2), (3)
366 a remarkably high pollution period lasting for four days (Stage 3), (4) an abruptly cleaned up period (Stage 4), and (5) another
367 clean period as the start of a new cycle (Stage 5). As shown in Fig. 10, each stage was initiated by a sudden change in the WD
368 and air masses from different regions via the HYSPLIT back trajectories (Draxler and Rolph, 2013). This indicates that
369 meteorological changes are important driving forces during the evolution of haze episodes.

370 Stage 1 was characterized by high winds from the northwest, which brought clean air masses from Western Siberia.
371 Aerosols associated with this air mass origin were largely free of high anthropogenic emissions and appeared to be aged with
372 a high contribution of secondary species. Consistently, the CO concentration during stage 1 was relatively low. During stage
373 2, the WD changed and the WS was lower than 1 m s⁻¹. The air masses from the northern and southern areas of Handan were
374 influenced by high anthropogenic emissions in northern Hebei and Henan province, respectively. Thus, the PM₁ concentration
375 steadily increased during this stage, with an average of 164.6 µg/m³. Stage 3 was dominated by southerly and northerly winds
376 and really stagnant conditions with low WS. On December 23, air masses from the southern and northern areas of Hebei
377 circulated around Handan, leading to the accumulation of air pollutants including PM and CO. The average PM₁ concentration
378 during stage 3 was 500.1 µg/m³, with the hourly maximum reaching as high as 700.8 µg/m³, much higher than that observed
379 during the severe haze episode in Beijing in January 2013 (~300 µg/m³; Sun et al., 2014). Accompanied with a high CO
380 concentration (average of ~7 ppm) during stage 3, O₃ concentration remained at a very low level of almost zero and with
381 minimal diurnal variations, suggesting that gas-phase oxidation might not be a dominant mechanism for haze formation.
382 Moreover, stage 3 was characterized with high RH, exceeding 70% most of the time, which would promote the aqueous-phase
383 formation of secondary species. Indeed, a high mass fraction of secondary species, especially a notable increase in sulfate
384 contribution, was observed during stage 3. During stage 4, due to the return of cleaner air masses long transported from
385 northwest, air pollutant concentrations in Handan decreased dramatically and PM₁ concentration decreased from 443.7 µg/m³
386 to 34.1 µg/m³ within only 12 hours.

387 To further evaluate the influence of air mass origins on aerosol characteristics, we performed the cluster analysis of
388 HYSPLIT back trajectories for the whole study period to elucidate the relationship between aerosol concentration or
389 composition and different clusters. As shown in Fig. S12, the whole NCP region was heavily polluted, with high PM₁
390 concentrations for all four clusters. Overall, the aerosol compositions were similar among different clusters. However, we

391 indeed observed an important role played by winds in altering aerosol characteristics according to the above case study.
392 Referring to the haze cycle analysis, we attempted to apply another classification method based on WD and WS. Periods with
393 WS exceeding 1.5 m s^{-1} from the northwest of Handan were denoted as “NW_HWS”, whereas the remaining periods were
394 classified as “Others” (Fig. 11). As expected, the PM_{10} concentration of “Others” was more than six times higher than that of
395 “NW_HWS”. Secondary aerosol species (i.e. sulfate, nitrate, ammonium and OOA) contributed 66% of total PM_{10} for
396 “NW_HWS”. As air masses associated with “Others” were more strongly influenced by anthropogenic sources, the main
397 primary species (i.e. HOA, BBOA, CCOA and BC), accounted for a higher fraction of 32% for “Others”. These results
398 highlight the importance of high winds from the northwest of Handan in alleviating PM levels and changing aerosol
399 composition during wintertime.

400 As mentioned previously, the sulfate contribution during stage 3 was visibly enhanced under high RH, revealing the
401 effects of RH on aerosol processing. Many previous studies have observed the increased production of secondary inorganic
402 aerosol species through aqueous-phase processing. In this study, we used the oxidation ratios of sulfur and nitrogen, defined
403 as $f_S = n\text{SO}_4^{2-} / (n\text{SO}_4^{2-} + n\text{SO}_2)$ and $f_N = n\text{NO}_3^- / (n\text{NO}_3^- + n\text{NO}_x)$, respectively, to explore the influence of RH on
404 aerosol formation (Fig. 12). Under relatively dry conditions ($\text{RH} < 50\%$), both f_S and f_N were almost constant. However,
405 when $\text{RH} > 50\%$, f_S started to increase linearly, similar to the results observed by Zheng et al. (2015) in Beijing. In comparison,
406 f_N showed a small increase at RH 60-70% and then decreased a bit when RH > 90%. ~~increased with a much slower speed,~~
407 suggesting different roles of aqueous-phase reactions in the formation of sulfate and nitrate. Recently, studies of aqueous-phase
408 chemistry have paid increasing attention to organic components. Ge et al. (2012) observed the strong enhancement of SOA
409 during a fog event in the Central Valley of California during winter. Based on high resolution mass spectra from an AMS, Sun
410 et al. (2016a) retrieved an aqueous-phase-processed SOA (aq-OOA) that tracked well with RH in Beijing during wintertime.
411 However, the mass fraction of SOA in total OA in this study remained relatively stable and showed no dependency on RH (Fig.
412 12c). The RH-binned bulk composition of submicron aerosol also only exhibited an obvious increase of sulfate at high RH
413 (Fig. S13). One explanation for this observation is that the variations of SOA contribution may be largely interfered by high
414 fractions of POA across different RH values. Another explanation is that, ~~For another,~~ a portion of OOA formed through
415 aqueous phase reactions may be incorporated into fog droplets, which are too large to be transmitted into the ACSM
416 aerodynamic lens, as reported by Ge et al. (2012). This explanation is consistent with the results obtained by studying a fog
417 event in London, in which no increase in OOA concentration was detected by AMS measurement, whereas the single particle
418 mass spectrometry observed aqueous-phase SOA production (Dall’Osto et al., 2009).

419 4 Conclusions

420 To characterize aerosol sources and formation processes under high anthropogenic emissions in the NCP region, a field
421 campaign was conducted in Handan during the extremely polluted winter of 2015-2016. For the entire study period, only 13
422 out of 65 days met the Chinese NAAQS Grade II of $75 \mu\text{g}/\text{m}^3$ for daily $\text{PM}_{2.5}$. The average concentration of submicron aerosol

423 was $187.6 \mu\text{g}/\text{m}^3$, with hourly values fluctuating dramatically by a factor of ~ 150 , from $4.2 \mu\text{g}/\text{m}^3$ to $700.8 \mu\text{g}/\text{m}^3$. Organics
424 dominated the bulk composition of submicron aerosols (44.6% of PM_{10} mass), similar to previous observations in the NCP
425 region during wintertime. PMF analysis identified three primary sources of organic aerosol, i.e. traffic, coal combustion and
426 biomass burning, and one SOA factor. CCOA was the largest contributor to POA, on average accounting for 29%, followed
427 by BBOA (25%). The mass fraction of HOA in total OA was only 7%, indicating the minor contribution of traffic emissions
428 in Handan. Although the aerosol concentration during polluted days was more than three times higher than that during non-
429 polluted days, little variation was observed in the average aerosol bulk composition, revealing the relatively synchronous
430 increase of all aerosol species during haze evolution. Stagnant weather conditions, with low wind speed and high RH, and
431 strong enhancement of primary species at nighttime, prompted haze formation during polluted days. Variation of aerosol mass
432 fractions with hourly increasing PM_{10} concentration further revealed that secondary formation of sulfate (mainly from SO_2
433 emitted by coal combustion) and primary emissions from coal combustion and biomass burning, are important factors driving
434 haze formation. This is mainly related to large emissions of air pollutants from coal and biomass combustion during wintertime,
435 especially for simple household stoves with low combustion efficiency. ~~the low efficient combustion of coal and biomass fuels~~
436 ~~during wintertime.~~ Overall, sulfate, chloride, and CCOA on average accounted for a total of 37% of PM_{10} mass (Fig. 1c),
437 showing the important role of coal combustion in air pollution in Handan. Given the continuing high consumption of coal for
438 various industries and residential heating in winter, technology-based emission controls on coal combustion would effectively
439 improve the air quality in Handan.

440 A severe haze episode that started with a steady build-up of aerosol pollution followed by an abrupt clean period was
441 studied. Our results indicate the strong influence of meteorological conditions on haze evolution. With high anthropogenic
442 emissions around Handan, the whole study region was heavily polluted. However, high aerosol loadings can be rapidly
443 alleviated by strong winds from the northwestern~~northeastern~~. Under high RH ($\text{RH} > 50\%$), the oxidation ratio of sulfur
444 increased linearly, suggesting the important role of aqueous phase chemistry in sulfate formation during wintertime. Results
445 from this study provide useful insights into aerosol chemistry and haze evolution in Hebei province during wintertime, and
446 have important implications for pollution control in this heavily polluted area.

447 **Acknowledgements**

448 This work was funded by the National Natural Science Foundation of China (41571130035 and 41625020) and the Ford
449 Company. Haiyan Li was partially supported by the Doctoral Short-Term Visiting-Abroad Foundation of Tsinghua University,
450 Beijing. Qi Zhang acknowledges the Changjiang Scholars program of the Chinese Ministry of Education. We also give special
451 acknowledgement to lab members in the Department of Environmental Engineering, Hebei University of Engineering, Handan,
452 China, whose help was invaluable in setting up this field campaign.

453 **References**

- 454 Aiken, A. C., Salcedo, D., Cubison, M. J., Huffman, J. A., DeCarlo, P. F., Ulbrich, I. M., Docherty, K. S., Sueper, D., Kimmel,
455 J. R., Worsnop, D. R., Trimborn, A., Northway, M., Stone, E. A., Schauer, J. J., Volkamer, R. M., Fortner, E., de Foy, B.,
456 Wang, J., Laskin, A., Shutthanandan, V., Zheng, J., Zhang, R., Gaffney, J., Marley, N. A., Paredes-Miranda, G., Arnott, W.
457 P., Molina, L. T., Sosa, G., and Jimenez, J. L.: Mexico City aerosol analysis during MILAGRO using high resolution aerosol
458 mass spectrometry at the urban supersite (T0) – Part 1: Fine particle composition and organic source apportionment, *Atmos.*
459 *Chem. Phys.*, 9, 6633–6653, doi:10.5194/acp-9-6633-2009, 2009.
- 460 Alfarra, M. R., Prévôt, A. S. H., Szidat, S., Sandradewi, J., Weimer, S., Lanz, V. A., Schreiber, D., Mohr, M., and Baltensperger,
461 U.: Identification of the mass spectral signature of organic aerosols from wood burning emissions, *Environ. Sci. Technol.*, 41,
462 5770– 5777, 2007.
- 463 Andreae, M. O., Schmid, O., Yang, H., Chand, D., Yu, J. Z., Zeng, L. M., and Zhang, Y. H.: Optical properties and chemical
464 composition of the atmospheric aerosol in urban Guangzhou, China, *Atmos. Environ.*, 42, 6335–6350, 2008.
- 465 [Baek, B. H., Koziel, J., and Aneja, V. P.: A preliminary review of gas-to-particle conversion, monitoring, and modeling efforts](#)
466 [in the USA. *Int. J. Global Environ. Iss.*, 6 \(2/3\), 204–230, 2006.](#)
- 467 Canonaco, F., Crippa, M., Slowik, J. G., Baltensperger, U., and Prévôt, A. S. H.: SoFi, an Igor based interface for the efficient
468 use of the generalized multilinear engine (ME-2) for source apportionment: application to aerosol mass spectrometer data,
469 *Atmos. Meas. Tech.*, 6 3649–3661, doi:10.5194/amt-6-3649-2013, 2013.
- 470 Cao, G., Zhang, X., and Zheng, F.: Inventory of black carbon and organic carbon emissions from China, *Atmos. Environ.*, 40,
471 6516–6527, 2006.
- 472 Carslaw, D. C. and Ropkins, K.: openair - An R package for air quality data analysis, *Environmental Modelling & Software*,
473 27-500 28, 52-61, 2012.
- 474 Crippa, M., Canonaco, F., Lanz, V. A., Äijälä, M., Allan, J. D., Carbone, S., Capes, G., Ceburnis, D., Dall’Osto, M., Day, D.
475 A., DeCarlo, P. F., Ehn, M., Eriksson, A., Freney, E., Hildebrandt Ruiz, L., Hillamo, R., Jimenez, J. L., Junninen, H., Kiendler-
476 Scharr, A., Kortelainen, A.-M., Kulmala, M., Laaksonen, A., Mensah, A. A., Mohr, C., Nemitz, E., O’Dowd, C., Ovadnevaite,
477 J., Pandis, S. N., Petäjä, T., Poulain, L., Saarikoski, S., Sellegri, K., Swietlicki, E., Tiitta, P., Worsnop, D. R., Baltensperger, U.,
478 and Prévôt, A. S. H.: Organic aerosol components derived from 25 AMS data sets across Europe using a consistent ME-2 based
479 source apportionment approach, *Atmos. Chem. Phys.*, 14, 6159– 6176, doi:10.5194/acp-14-6159-2014, 2014.
- 480 Dall’Osto, M., Harrison, R. M., Coe, H., and Williams, P.: Real-time secondary aerosol formation during a fog event in London,
481 *Atmos. Chem. Phys.*, 9, 2459-2469, doi:10.5194/acp-9-2459-2009, 2009.
- 482 Ding, J., Zhong, J., Yang, Y., Li, B., Shen, G., Su, Y., Wang, C., Li, W., Shen, H., Wang, B., Wang, R., Huang, Y., Zhang, Y.,
483 Cao, H., Zhu, Y., Simonich, S.L., and Tao, S.: Occurrence and exposure to polycyclic aromatic hydrocarbons and their
484 derivatives in a rural Chinese home through biomass fuelled cooking, *Environ. Pollut.*, 169, 160–166, 2012.
- 485 Draxler, R. R. and Rolph, G.D.: HYSPLIT (Hybrid single-particle lagrangian integrated trajectory) Model access via NOAA

486 ARL READY Website, available at: <http://www.arl.noaa.gov/HYSPLIT.php> (last access: 2014), NOAA Air Resources
487 Laboratory, College Park, MD, 2013.

488 Elser, M., Huang, R.-J., Wolf, R., Slowik, J. G., Wang, Q., Canonaco, F., Li, G., Bozzetti, C., Daellenbach, K. R., Huang, Y.,
489 Zhang, R., Li, Z., Cao, J., Baltensperger, U., El-Haddad, I., and Prévôt, A. S. H.: New insights into PM_{2.5} chemical
490 composition and sources in two major cities in China during extreme haze events using aerosol mass spectrometry, *Atmos.*
491 *Chem. Phys.*, 16, 3207-3225, doi:10.5194/acp-16-3207-2016, 2016.

492 Ge, X. L., Zhang, Q., Sun, Y. L., Ruehl, C. R., and Setyan, A.: Effect of aqueous-phase processing on aerosol chemistry and
493 size distributions in Fresno, California, during wintertime, *Environ. Chem.*, 9, 221–235, doi:10.1071/EN11168, 2012.

494 [Guo, S., Hu, M., Zamora, M. L., Peng, J. F., Shang, D. J., Zheng, J., Du, Z. F., Wu, Z., Shao, M., Zeng, L. M., Molina, M. J.,](#)
495 [and Zhang, R. Y.: Elucidating severe urban haze formation in China, *P Natl Acad Sci USA*, 111, 17373-17378,](#)
496 [10.1073/pnas.1419604111, 2014.](#)

497 Hu, W. W., Hu, M., Yuan, B., Jimenez, J. L., Tang, Q., Peng, J. F., Hu, W., Shao, M., Wang, M., Zeng, L. M., Wu, Y. S., Gong,
498 Z. H., Huang, X. F., and He, L. Y.: Insights on organic aerosol aging and the influence of coal combustion at a regional receptor
499 site of central eastern China, *Atmos. Chem. Phys.*, 13, 10095-10112, doi:10.5194/acp-13-10095-2013, 2013.

500 Hu, W., Hu, M., Hu, W., Jimenez, J. L., Yuan, B., Chen, W., Wang, M., Wu, Y., Chen, C., Wang, Z., Peng, J., Zeng, L., and
501 Shao, M.: Chemical composition, sources and aging process of submicron aerosols in Beijing: contrast between summer and
502 winter, *J. Geophys. Res.*, 121, 1955–1977, doi:10.1002/2015JD024020, 2016.

503 Huang, R.-J., Zhang, Y., Bozzetti, C., Ho, K.-F., Cao, J.-J., Han, Y., Daellenbach, K. R., Slowik, J.G., Platt, S. M., Canonaco,
504 F., Zotter, P., Wolf, R., Pieber, S. M., Bruns, E. A., Crippa, M., Ciarelli, G., Piazzalunga, A., Schwikowski, M., Abbaszade, G.,
505 SchnelleKreis, J., Zimmermann, R., An, Z., Szidat, S., Baltensperger, U., El Haddad, I., and Prévôt, A. S. H.: High secondary
506 aerosol contribution to particulate pollution during haze events in China, *Nature*, 514, 218–222, doi:10.1038/nature13774,
507 2014.

508 Jia, Y. T., Rahn, K. A., He, K. B., Wen, T. X., and Wang, Y. S.: A novel technique for quantifying the regional component of
509 urban aerosol solely from its sawtooth cycles, *J. Geophys. Res.*, 113, D21309, doi:10.1029/2008JD010389, 2008. Kim, H.,
510 Zhang, Q., Bae, G.-N., Kim, J. Y., and Lee, S. B.: Sources and atmospheric processing of wintertime aerosols in Seoul, Korea:
511 Insights from real-time measurements using a high-resolution aerosol mass spectrometer, *Atmos. Chem. Phys. Discuss.*,
512 doi:10.5194/acp-2016-855, in review, 2016.

513 Lanz, V. A., Alfarra, M. R., Baltensperger, U., Buchmann, B., Hueglin, C., and Prévôt, A. S. H.: Source apportionment of
514 submicron organic aerosols at an urban site by factor analytical modelling of aerosol mass spectra, *Atmos. Chem. Phys.*, 7,
515 1503-1522, doi:10.5194/acp-7-1503-2007, 2007.

516 Lee, T., Sullivan, A. P., Mack, L., Jimenez, J. L., Kreidenweis, S. M., Onasch, T. B., Worsnop, D. R., Malm, W., Wold, C. E.,
517 Hao, W. M., and Collett, J. L.: Variation of chemical smoke marker emissions during flaming vs. smoldering phases of
518 laboratory open burning of wildland fuels, *Aerosol Sci. Technol.*, 44, 1–5, doi:10.1080/02786826.2010.499884, 2010.

519 Li, H., Zhang, Q., Duan, F., Zheng, B., and He, K.: The “Parade Blue”: effects of short-term emission control on aerosol
520 chemistry, *Faraday Discuss.*, 189, 317-335, 2016a.

521 Li, H., Duan, F., He, K., Ma, Y., Kimoto, T., Huang, T.: Size-dependent characterization of atmospheric particles during winter
522 in Beijing, *Atmosphere*, 7, 2016b.

523 [Lobert, J. M., Keene, W. C., Logan, J. A., and Yevich, R.: Global chlorine emissions from biomass burning: Reactive Chlorine](#)
524 [Emissions Inventory, *J Geophys Res-Atmos*, 104, 8373-8389, Doi 10.1029/1998jd100077, 1999.](#)

525 Mader, B. T., and Pankow, J. F.: Study of the effects of particle-phase carbon on the gas/particle partitioning of semivolatile
526 organic compounds in the atmosphere using controlled field experiments. *Environ. Sci. Technol.*, 36, 5218-5228, 2002.

527 [McCulloch, A., Aucott, M. L., Benkovitz, C. M., Graedel, T. E., Kleiman, G., Midgley, P. M., and Li, Y. F.: Global emissions](#)
528 [of hydrogen chloride and chloromethane from coal combustion, incineration and industrial activities: Reactive Chlorine](#)
529 [Emissions Inventory, *J Geophys Res-Atmos*, 104, 8391-8403, Doi 10.1029/1999jd900025, 1999.](#)

530 Middlebrook, A. M., Bahreini, R., Jimenez, J. L., and Canagaratna, M. R.: Evaluation of Composition-Dependent Collection
531 Efficiencies for the Aerodyne Aerosol Mass Spectrometer using Field Data, *Aerosol Sci. Tech.*, 46, 258–271, 2012.

532 Ng, N. L., Canagaratna, M. R., Zhang, Q., Jimenez, J. L., Tian, J., Ulbrich, I. M., Kroll, J. H., Docherty, K. S., Chhabra, P. S.,
533 Bahreini, R., Murphy, S. M., Seinfeld, J. H., Hildebrandt, L., Donahue, N. M., DeCarlo, P. F., Lanz, V. A., Prévôt, A. S. H.,
534 Dinar, E., Rudich, Y., and Worsnop, D. R.: Organic aerosol components observed in Northern Hemispheric datasets from
535 Aerosol Mass Spectrometry, *Atmos. Chem. Phys.*, 10, 4625-4641, doi:10.5194/acp-10-4625-2010, 2010.

536 Ng, N. L., Herndon, S. C., Trimborn, A., Canagaratna, M. R., Croteau, P., Onasch, T. M., Sueper, D., Worsnop, D. R., Zhang,
537 Q., Sun, Y. L., and Jayne, J. T.: An Aerosol Chemical Speciation Monitor (ACSM) for routine monitoring of atmospheric
538 aerosol composition, *Aerosol Sci. Technol.*, 45, 770–784, 2011a.

539 Ng, N. L., Canagaratna, M. R., Jimenez, J. L., Zhang, Q., Ulbrich, I. M., and Worsnop, D. R.: Real-time methods for estimating
540 organic component mass concentrations from aerosol mass spectrometer data, *Environ. Sci. Technol.*, 45, 910–916, 2011b.

541 Ng, N. L., Canagaratna, M. R., Jimenez, J. L., Chhabra, P. S., Seinfeld, J. H., and Worsnop, D. R.: Changes in organic aerosol
542 composition with aging inferred from aerosol mass spectra, *Atmos. Chem. Phys.*, 11, 6465-6474, doi:10.5194/acp-11-6465-
543 2011, 2011c.

544 Paatero, P. and Tapper, U.: Positive Matrix Factorization: a non-negative factor model with optimal utilization of error
545 estimates of data values, *Environmetrics*, 5, 111–126, 1994.

546 Paatero, P.: The multilinear engine - A table-driven, least squares program for solving multilinear problems, including the n-
547 way parallel factor analysis model, *J. Comput. Graph. Stat.*, 8, 854– 888, 1999.

548 Petzold, A. and Schonlinner, M.: Multi-angle absorption photometry – a new method for the measurement of aerosol light
549 absorption and atmospheric black carbon, *J. Aerosol Sci.*, 35, 421–441, 2004.

550 Petzold, A., Schloesser, H., Sheridan, P. J., Arnott, W. P., Ogren, J. A., and Virkkula, A.: Evaluation of multiangle absorption
551 photometry for measuring aerosol light absorption, *Aerosol Sci. Tech.*, 39, 40–51, 2005.

552 Pope III, C. A. and Dockery, D. W.: Health Effects of Fine Particulate Air Pollution: Lines that Connect, *J. Air Waste Manage.*

553 56, 709–742, 2006.

554 Pöschl, U.: Atmospheric Aerosols: Composition, Transformation, Climate and Health Effects, *Angew. Chem. Int. Ed.*, 44,
555 7520–7540, 2005.

556 Quan, J., Tie, X., Zhang, Q., Liu, Q., Li, X., Gao, Y., and Zhao, D.: Characteristics of heavy aerosol pollution during the 2012–
557 2013 winter in Beijing, China, *Atmos. Environ.*, 88, 83–89, doi:10.1016/j.atmosenv.2014.01.058, 2014.

558 Ramanathan, V., Crutzen, P. J., Kiehl, J. T., and Rosenfeld, D.: Aerosols, climate and the hydrological cycle, *Science*, 294,
559 2119–2124, 2001.

560 Regalado J, Pérez-Padilla R, Sansores R, Ramirez JIP, Brauer M, Paré P, and Vedal, S.: The effect of biomass burning on
561 respiratory symptoms and lung function in rural Mexican women. *Am J Respir Crit Care Med.*, 174, 901–905, 2006.

562 Seinfeld, J. H. and Pandis, S. N.: *Atmospheric Chemistry and Physics: From Air Pollution to Climate Change*, John Wiley &
563 Sons, New York, 2nd edition, 1232 pp., ISBN-13: 978-0-471-72018-8, 2006.

564 Sun, J. Y., Zhang, Q., Canagaratna, M. R., et al.: Highly time- and size-resolved characterization of submicron aerosol particles
565 in Beijing using an Aerodyne Aerosol Mass Spectrometer, *Atmos. Environ.*, 44, 131–140, 2010.

566 Sun, Y., Wang, Z., Dong, H., Yang, T., Li, J., Pan, X., Chen, P., and Jayne, J. T.: Characterization of summer organic and
567 inorganic aerosols in Beijing, China with an Aerosol Chemical Speciation Monitor, *Atmos. Environ.*, 51, 250–259,
568 doi:10.1016/j.atmosenv.2012.01.013, 2012.

569 Sun, Y. L., Wang, Z. F., Fu, P. Q., Yang, T., Jiang, Q., Dong, H. B., Li, J., and Jia, J. J.: Aerosol composition, sources and
570 processes during wintertime in Beijing, China, *Atmos. Chem. Phys.*, 13, 4577–4592, doi:10.5194/acp-13-4577-2013, 2013a.

571 Sun, Y. L., Wang, Z. F., Fu, P. Q., Jiang, Q., Yang, T., Li, J., and Ge, X. L.: The impact of relative humidity on aerosol
572 composition and evolution processes during wintertime in Beijing, China, *Atmos. Environ.*, 77, 927–934,
573 doi:10.1016/j.atmosenv.2013.06.019, 2013b.

574 Sun, Y., Jiang, Q., Wang, Z., Fu, P., Li, J., Yang, T., and Yin, Y.: Investigation of the Sources and Evolution Processes of Severe
575 Haze Pollution in Beijing in January 2013, *J. Geophys. Res.*, 119, 4380–4398, 2014.

576 Sun, Y. L., Wang, Z. F., Du, W., Zhang, Q., Wang, Q. Q., Fu, P. Q., Pan, X. L., Li, J., Jayne, J., and Worsnop, D. R.: Long-term
577 real-time measurements of aerosol particle composition in Beijing, China: seasonal variations, meteorological effects, and
578 source analysis, *Atmos. Chem. Phys.*, 15, 10149–10165, doi:10.5194/acp-15-10149-2015, 2015.

579 Sun, Y., Du, W., Fu, P., Wang, Q., Li, J., Ge, X., Zhang, Q., Zhu, C., Ren, L., Xu, W., Zhao, J., Han, T., Worsnop, D. R., and
580 Wang, Z.: Primary and secondary aerosols in Beijing in winter: sources, variations and processes, *Atmos. Chem. Phys.*, 16,
581 8309–8329, doi:10.5194/acp-16-8309-2016, 2016a.

582 Sun, Y., Jiang, Q., Xu Y., Ma, Y., Zhang, Y., Liu, X., Li, W., Wang, F., Li, J., Wang, P., and Li, Z.: Aerosol characterization
583 over the North China Plain: Haze life cycle and biomass burning impacts in summer, *J. Geophys. Res. Atmos.*, 121, 2508–
584 2521, doi:10.1002/2015JD024261, 2016b.

585 Takegawa, N., Miyakawa, T., Kuwata, M., et al.: Variability of submicron aerosol observed at a rural site in Beijing in the
586 summer of 2006, *J. Geophys. Res.*, 114, D00G05, doi:10.1029/2008JD010857, 2009.

587 Ulbrich, I. M., Canagaratna, M. R., Zhang, Q., Worsnop, D. R., and Jimenez, J. L.: Interpretation of organic components from
588 Positive Matrix Factorization of aerosol mass spectrometric data, *Atmos. Chem. Phys.*, 9, 2891-2918, doi:10.5194/acp-9-2891-
589 2009, 2009.

590 Wang, G., Cheng, S., Li, J., Lang, J., Wen, W., Yang, X., and Tian, L.: Source apportionment and seasonal variation of PM_{2.5}
591 carbonaceous aerosol in the Beijing–Tianjin–Hebei Region of China. *Environ. Monit. Assess.* 187, 2015.

592 Wang, L. T., Wei, Z., Yang, J., Zhang, Y., Zhang, F. F., Su, J., Meng, C. C., and Zhang, Q.: The 2013 severe haze over southern
593 Hebei, China: model evaluation, source apportionment, and policy implications, *Atmos. Chem. Phys.*, 14, 3151-3173,
594 doi:10.5194/acp-14-3151-2014, 2014.

595 Wang, X., Wang, W., Yang, L., Gao, X., Nie, W., Yu, Y., Xu, P., Zhou, Y., and Wang, Z.: The secondary formation of
596 inorganic aerosols in the droplet mode through heterogeneous aqueous reactions under haze conditions, *Atmos. Environ.*, 63,
597 68–76, 2012.

598 Wei, Z., Wang, L.T., Chen, M.Z., and Zheng, Y.: The 2013 severe haze over the Southern Hebei, China: PM_{2.5} composition
599 and source apportionment, *Atmos. Pollut. Res.* 5, 759-768, 2014.

600 Xu, J., Shi, J., Zhang, Q., Ge, X., Canonaco, F., Prévôt, A. S. H., Vonwiller, M., Szidat, S., Ge, J., Ma, J., An, Y., Kang, S.,
601 and Qin, D.: Wintertime organic and inorganic aerosols in Lanzhou, China: Sources, processes and comparison with the results
602 during summer, *Atmos. Chem. Phys. Discuss.*, doi:10.5194/acp-2016-278, in review, 2016.

603 Xu, L., Suresh, S., Guo, H., Weber, R. J., and Ng, N. L.: Aerosol characterization over the southeastern United States using
604 high-resolution aerosol mass spectrometry: spatial and seasonal variation of aerosol composition and sources with a focus on
605 organic nitrates, *Atmos. Chem. Phys.*, 15, 7307-7336, doi:10.5194/acp-15-7307-2015, 2015.

606 Yang, Y. R., Liu, X. G., Qu, Y., An, J. L., Jiang, R., Zhang, Y. H., Sun, Y. L., Wu, Z. J., Zhang, F., Xu, W. Q., and Ma, Q. X.:
607 Characteristics and formation mechanism of continuous hazes in China: a case study during the autumn of 2014 in the North
608 China Plain, *Atmos. Chem. Phys.*, 15, 8165-8178, doi:10.5194/acp-15-8165-2015, 2015.

609 Young, D. E., Kim, H., Parworth, C., Zhou, S., Zhang, X., Cappa, C. D., Seco, R., Kim, S., and Zhang, Q.: Influences of
610 emission sources and meteorology on aerosol chemistry in a polluted urban environment: results from DISCOVER-AQ
611 California, *Atmos. Chem. Phys.*, 16, 5427-5451, doi:10.5194/acp-16-5427-2016, 2016.

612 Zhang, J. K., Sun, Y., Liu, Z. R., Ji, D. S., Hu, B., Liu, Q., and Wang, Y. S.: Characterization of submicron aerosols during a
613 month of serious pollution in Beijing, 2013, *Atmos. Chem. Phys.*, 14, 2887-2903, doi:10.5194/acp-14-2887-2014, 2014.

614 Zhang, Q., Worsnop, D. R., Canagaratna, M. R., and Jimenez, J. L.: Hydrocarbon-like and oxygenated organic aerosols in
615 Pittsburgh: insights into sources and processes of organic aerosols, *Atmos. Chem. Phys.*, 5, 3289-3311, doi:10.5194/acp-5-
616 3289-2005, 2005a.

617 Zhang, Q., Alfarra, M. R., Worsnop, D. R., Allan, J. D., Coe, H., Canagaratna, M. R., and Jimenez, J. L.: Deconvolution and
618 quantification of hydrocarbon-like and oxygenated organic aerosols based on aerosol mass spectrometry, *Environ. Sci.*
619 *Technol.*, 39, 4938–4952, 2005b.

620 Zhang, Q., Jimenez, J. L., Canagaratna, M. R., Ulbrich, I. M., Ng, N. L., Worsnop, D. R., and Sun, Y.: Understanding

621 atmospheric organic aerosols via factor analysis of aerosol mass spectrometry: a review, *Anal. Bioanal. Chem.*, 401, 3045–
622 3067, 2011.

623 Zhang, R., Jing, J., Tao, J., Hsu, S.-C., Wang, G., Cao, J., Lee, C. S. L., Zhu, L., Chen, Z., Zhao, Y., and Shen, Z.: Chemical
624 characterization and source apportionment of PM_{2.5} in Beijing: seasonal perspective, *Atmos. Chem. Phys.*, 13, 7053-7074,
625 doi:10.5194/acp-13-7053-2013, 2013.

626 Zhang, Y., Dou, H., Chang, B., Wei, Z., Qiu, W., Liu, S., Liu, W., and Tao, S.: Emission of Polycyclic Aromatic Hydrocarbons
627 from Indoor Straw Burning and Emission Inventory Updating in China, *Annals of the New York Academy of Sciences*, 1140,
628 218–227, doi:10.1196/annals.1454.006, 2008a.

629 Zhang, Y., Schauer, J. J., Zhang, Y., Zeng, L., Wei, Y., Liu, Y., and Shao, M.: Characteristics of particulate carbon emissions
630 from real-world Chinese coal combustion, *Environ. Sci. Technol.*, 42, 5068–5073, 2008b.

631 Zhao, P. S., Dong, F., He, D., Zhao, X. J., Zhang, X. L., Zhang, W. Z., Yao, Q., and Liu, H. Y.: Characteristics of concentrations
632 and chemical compositions for PM_{2.5} in the region of Beijing, Tianjin, and Hebei, China, *Atmos. Chem. Phys.*, 13, 4631-4644,
633 doi:10.5194/acp-13-4631-2013, 2013.

634 Zheng, B., Zhang, Q., Zhang, Y., He, K. B., Wang, K., Zheng, G. J., Duan, F. K., Ma, Y. L., and Kimoto, T.: Heterogeneous
635 chemistry: a mechanism missing in current models to explain secondary inorganic aerosol formation during the January 2013
636 haze episode in North China, *Atmos. Chem. Phys.*, 15, 2031-2049, doi:10.5194/acp-15-2031-2015, 2015.

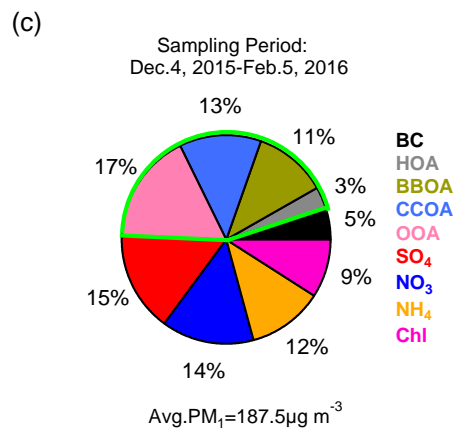
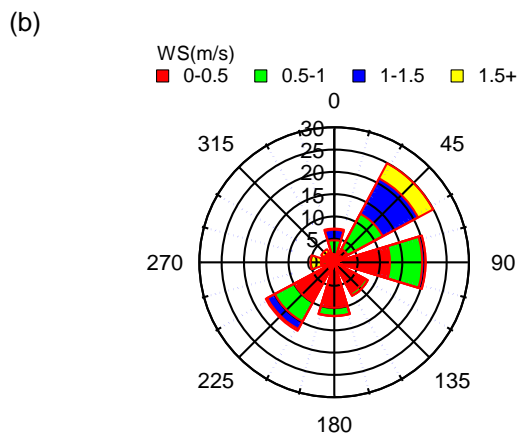
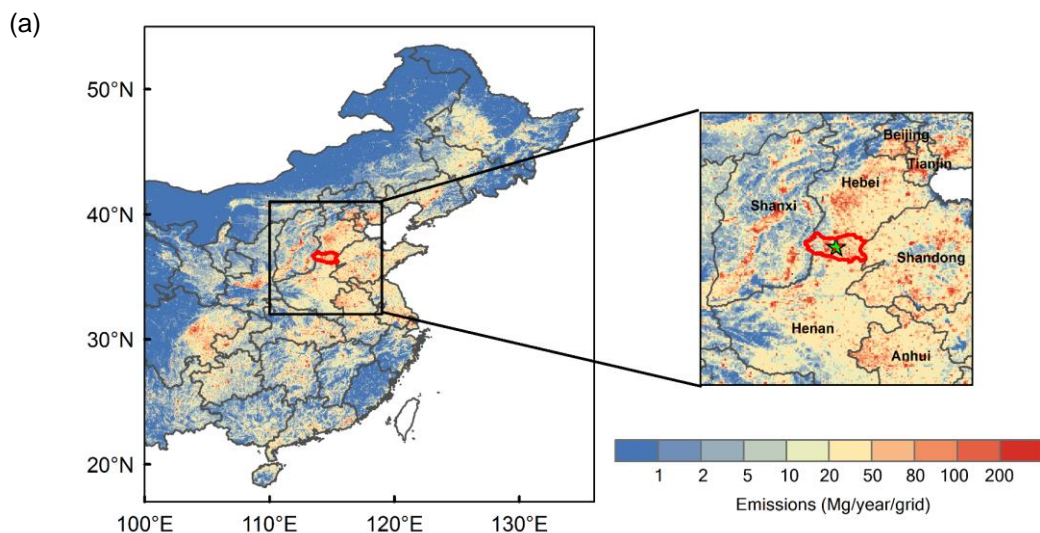
637 Zheng, G. J., Duan, F. K., Su, H., Ma, Y. L., Cheng, Y., Zheng, B., Zhang, Q., Huang, T., Kimoto, T., Chang, D., Pöschl, U.,
638 Cheng, Y. F., and He, K. B.: Exploring the severe winter haze in Beijing: the impact of synoptic weather, regional transport
639 and heterogeneous reactions, *Atmos. Chem. Phys.*, 15, 2969-2983, doi:10.5194/acp-15-2969-2015, 2015.

640 Zheng, G., Duan, F., Ma, Y., Zhang, Q., Huang, T., Kimoto, T., Cheng, Y., Su, H., and He, K.: Episode-Based Evolution Pattern
641 Analysis of Haze Pollution: Method Development and Results from Beijing, China, *Environ. Sci. Technol.*, 50, 4632–4641,
642 2016.

643 Zhou, S., Collier, S., Xu, J., Mei, F., Wang, J., Lee, Y. N., Sedlacek III, A. J., Springston, S. R., Sun, Y., and Zhang, Q.:
644 Influences of upwind emission sources and atmospheric processing on aerosol chemistry and properties at a rural location in
645 the Northeastern US, *J. Geophys. Res.*, 121, 6049–6065, doi:10.1002/2015JD024568., 2016.

646 Zhou, W., Jiang, J., Duan, L., and Hao, J.: Evolution of submicron organic aerosols during a complete residential coal
647 combustion process, *Environ. Sci. Technol.*, 50, 7861-7869, 2016.

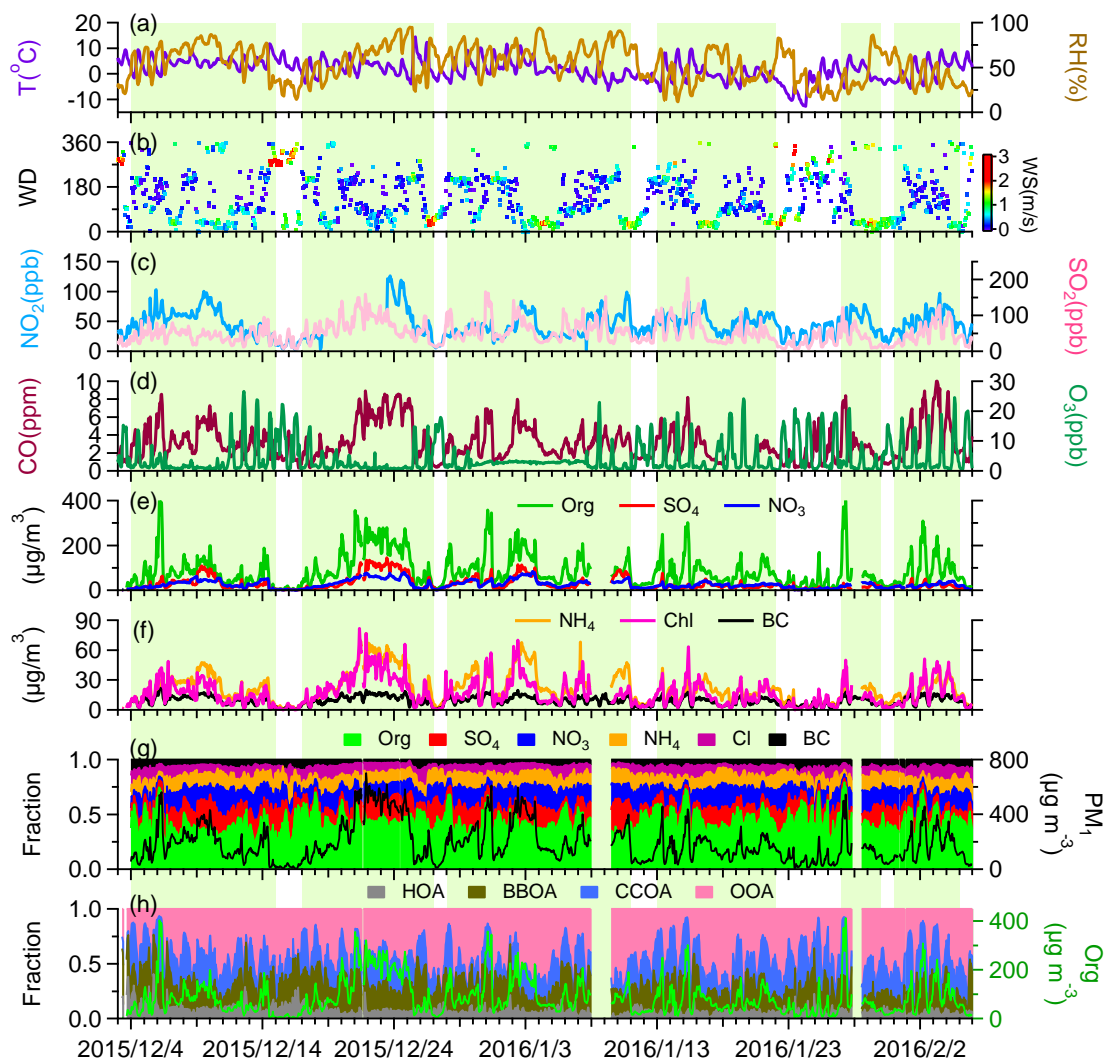
648



649

650 **Figure 1.** (a) Location of the sampling site in Handan in North China Plain. The map is color-coded by annual organic carbon emission
 651 rates modeled by Multi-resolution Emission Inventory for China (MEIC, <http://www.meicmodel.org>). The grid size is $0.05^\circ \times 0.05^\circ$. (b)
 652 Wind rose plot colored by wind speed for the entire period. Radial scales correspond to the frequency. (c) Compositional pie chart of
 653 submicron aerosol for the whole study, where the total organic fraction is outlined in green.

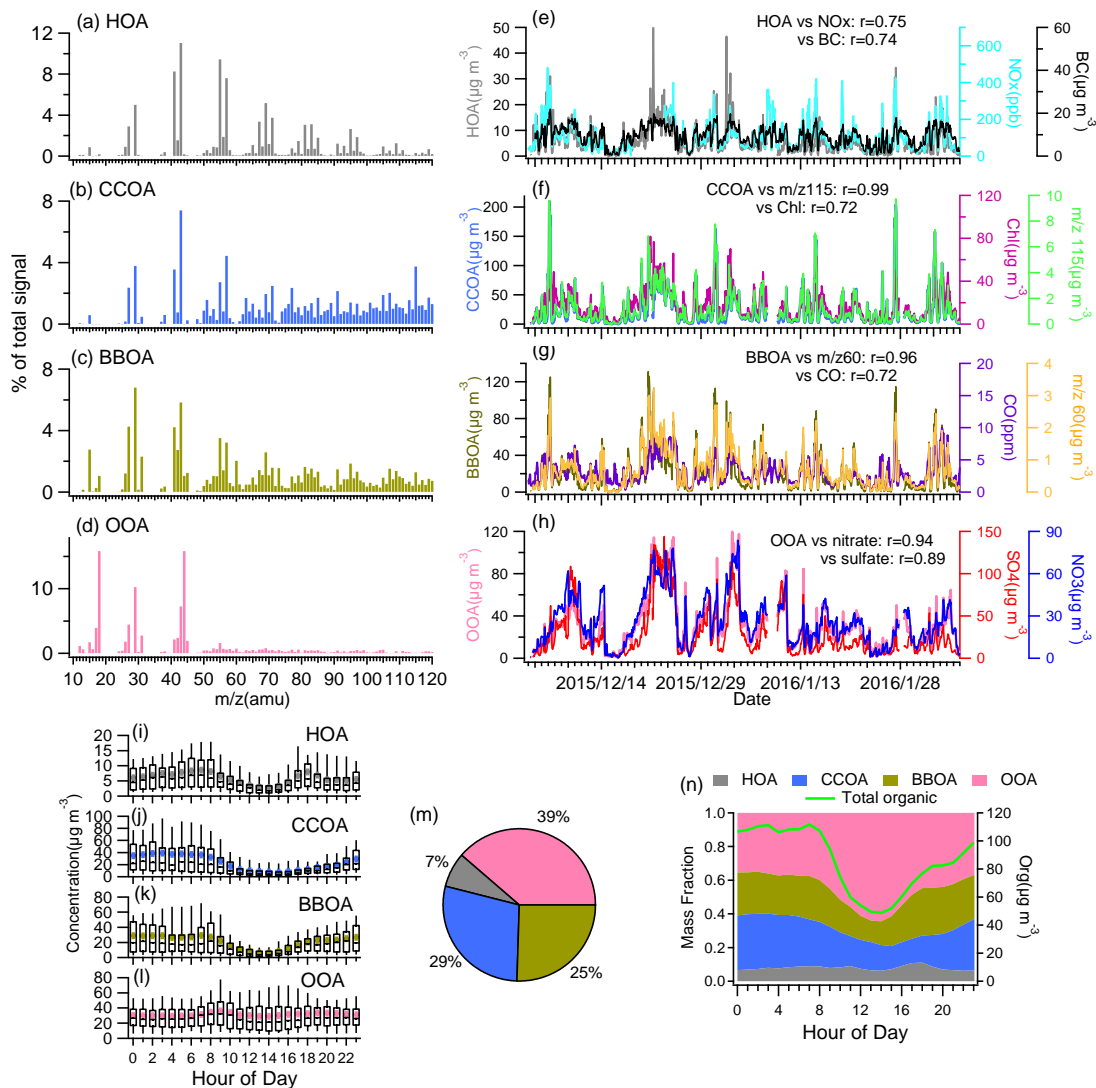
654



655

656 **Figure 2.** Time series of (a) ambient air temperature (T) and relative humidity (RH); (b) wind direction (WD) colored by wind speed
 657 (WS); (c) mixing ratios of NO₂ and SO₂; (d) mixing ratios of CO and O₃; (e) mass concentrations of organics, sulfate and nitrate; (f) mass
 658 concentrations of ammonium, chloride, and black carbon; (g) mass fractional contribution of chemical species to total PM₁ with the time
 659 series of total PM₁ concentration plotted in black on the right y-axis; (h) mass fractional contribution to total OA mass of the four factors
 660 derived from PMF analysis with the time series of organic aerosol plotted in green on the right y-axis. Days violating the CNAAQs for
 661 PM_{2.5} (= 75 µg m⁻³) are highlighted in pale green.

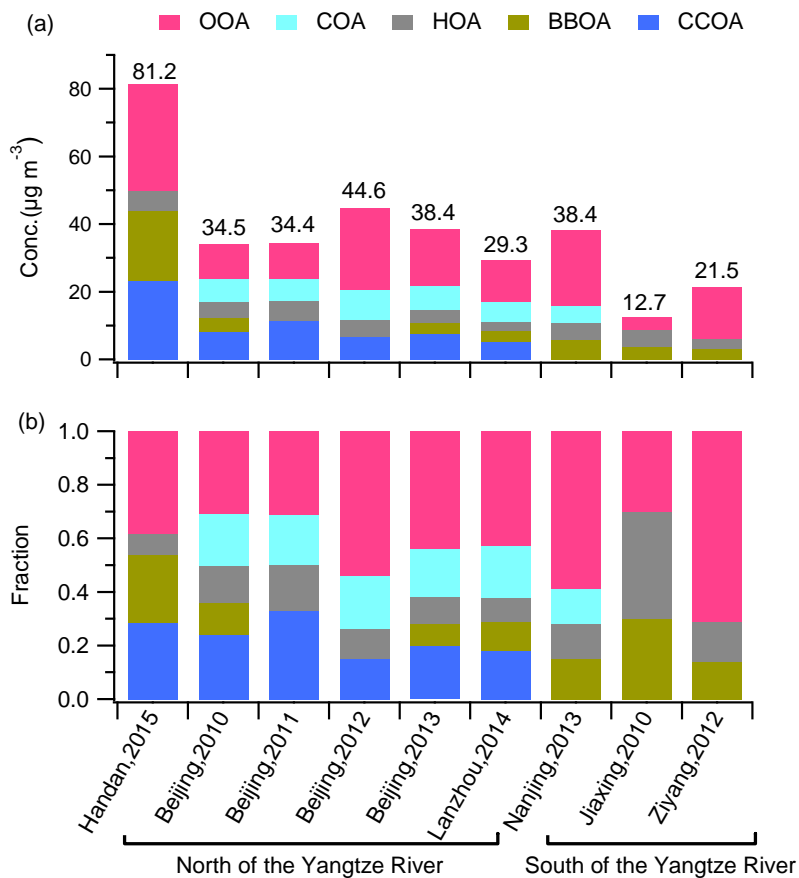
662



663

664 **Figure 3.** (a-d) Mass spectra of hydrocarbon-like OA (HOA), coal combustion OA (CCOA), biomass burning OA (BBOA), and
 665 oxygenated OA (OOA). (e-h) Time series of OA factors and the corresponding tracer compounds. (i-l) Diurnal patterns of OA factors. (m)
 666 Average fractional pie chart of OA factors to total OA for the campaign. (n) Average diurnal mass contributions of OA factors to total OA,
 667 with the average diurnal concentration of organics on the right y-axis.

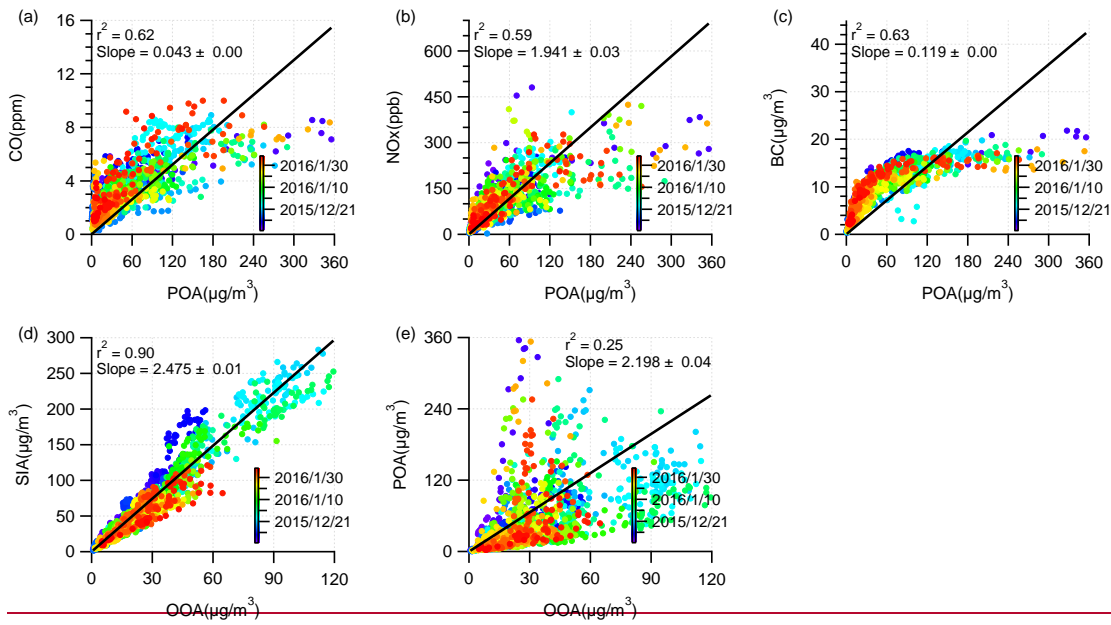
668



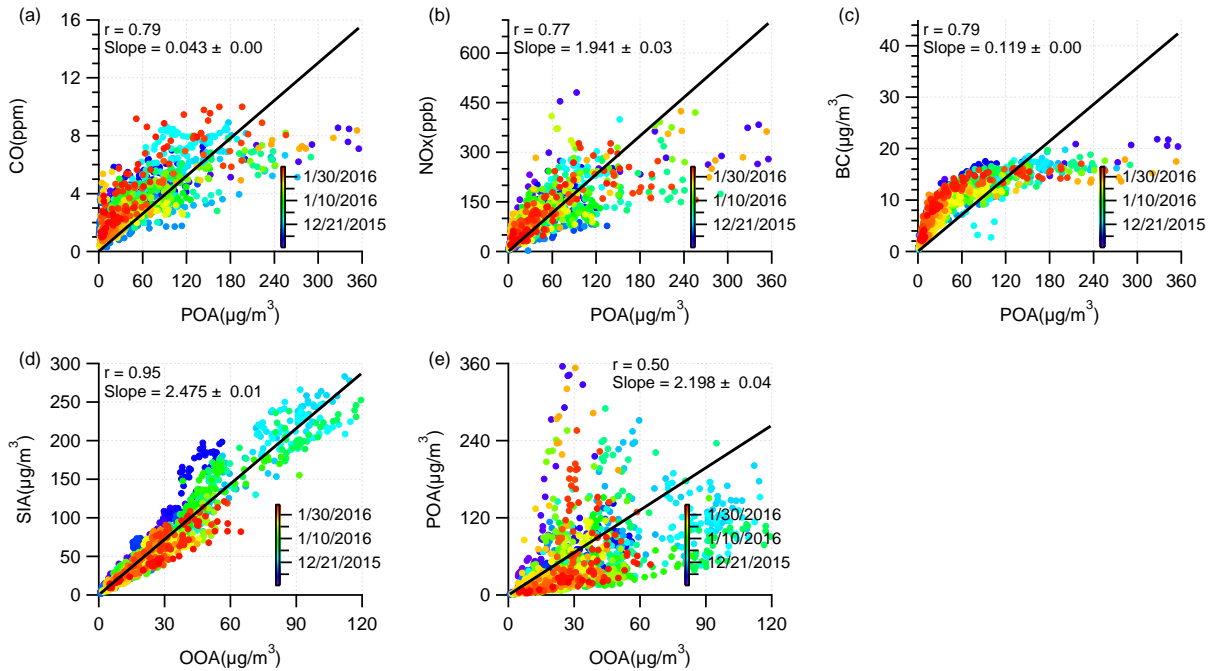
669

670 **Figure 4.** Summary of the average (a) mass concentration and (b) chemical composition of organic aerosols from winter
 671 studies in China. The total concentration of OA ($\mu\text{g}/\text{m}^3$) is shown on the top of the bar in panel (a). See Table S1 in the
 672 Supplement for detailed information.

673



674

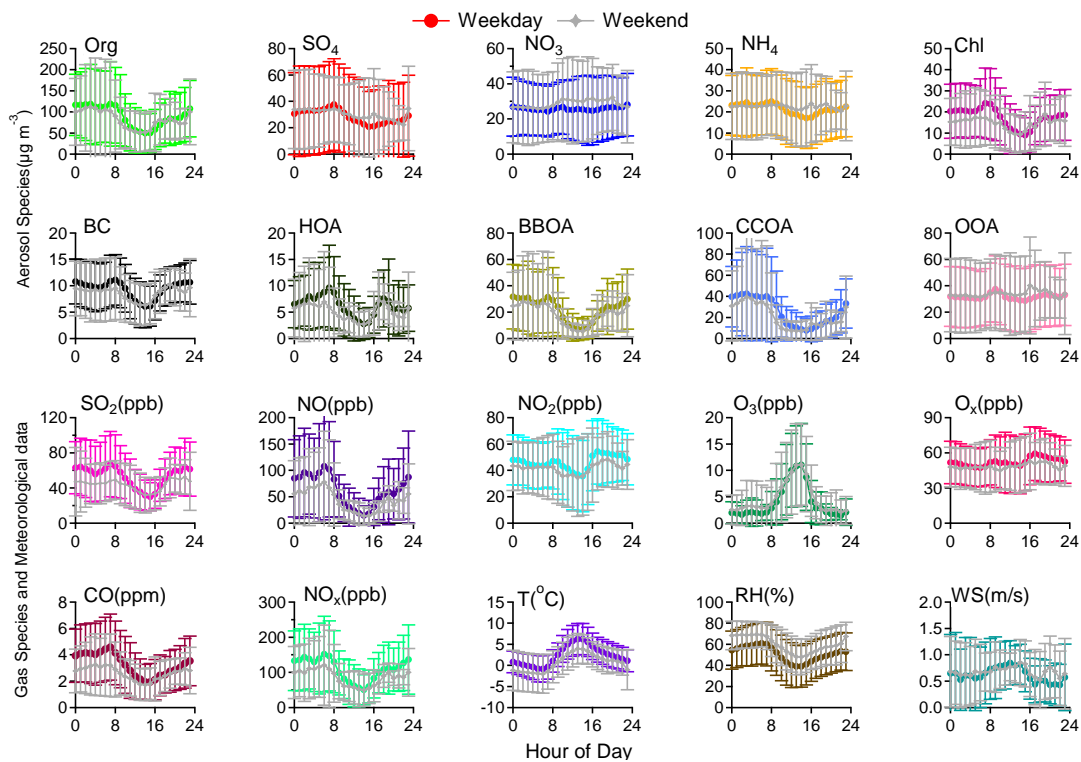


675

676

Figure 5. Scatter plots of (a) CO vs POA, (b) NO_x vs POA, (c) BC vs POA, (d) SIA vs OOA, and (e) POA vs OOA.

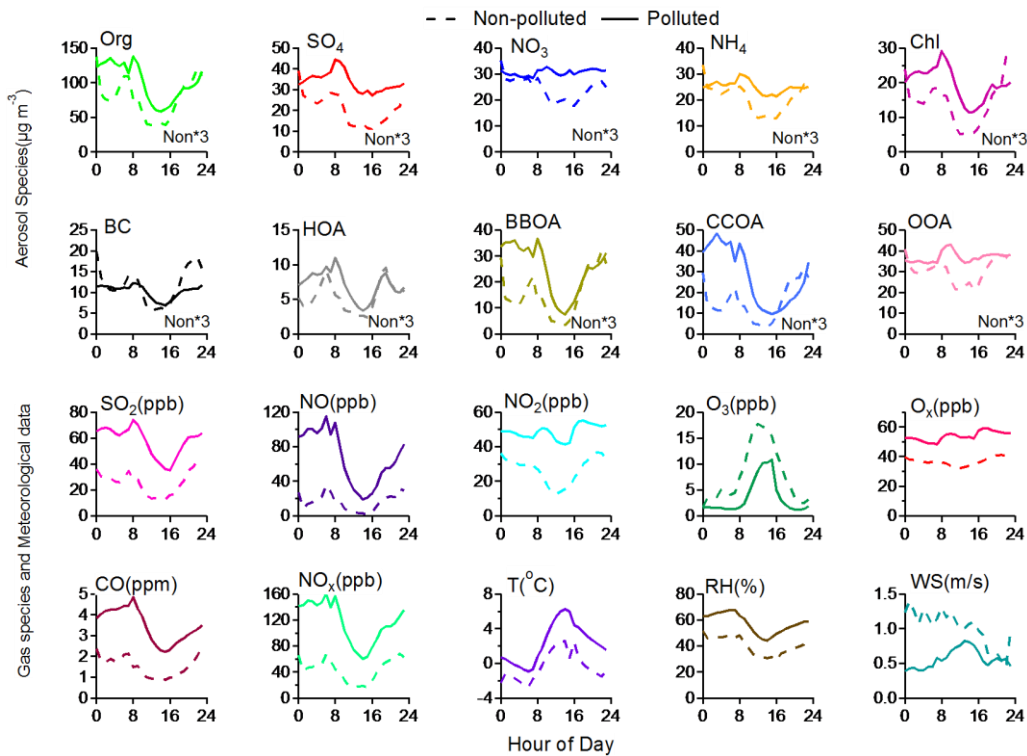
677



678

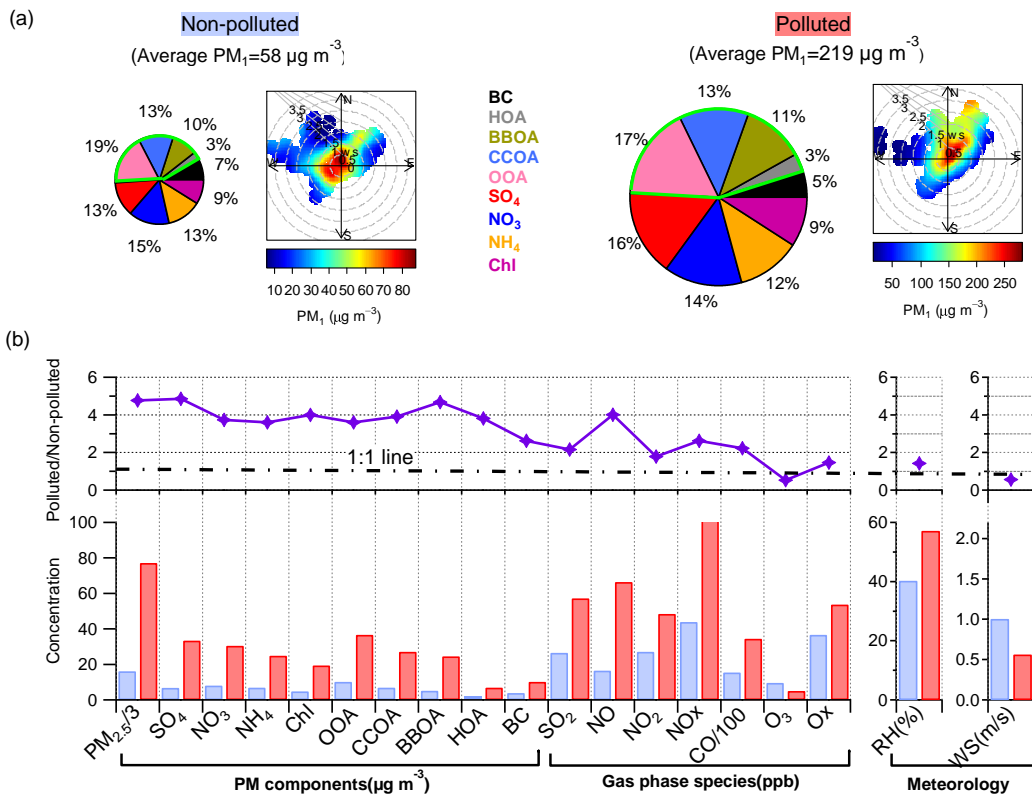
679 **Figure 6.** Average diurnal profiles along with the standard deviation of PM₁ species, four OA factors identified by PMF analysis, various
 680 gas-phase species, and meteorological parameters on weekdays (Tuesday to Friday inclusive) and weekends (Sunday only) during the
 681 campaign.

682



683
684
685
686

Figure 7. Average diurnal cycles of PM₁ species, four OA factors identified via PMF analysis, various gas-phase species, and meteorological parameters on polluted and non-polluted days. The mass concentrations of aerosol species during non-polluted periods are scaled by three factors in to highlight the differences in their diurnal trends on polluted and non-polluted days.



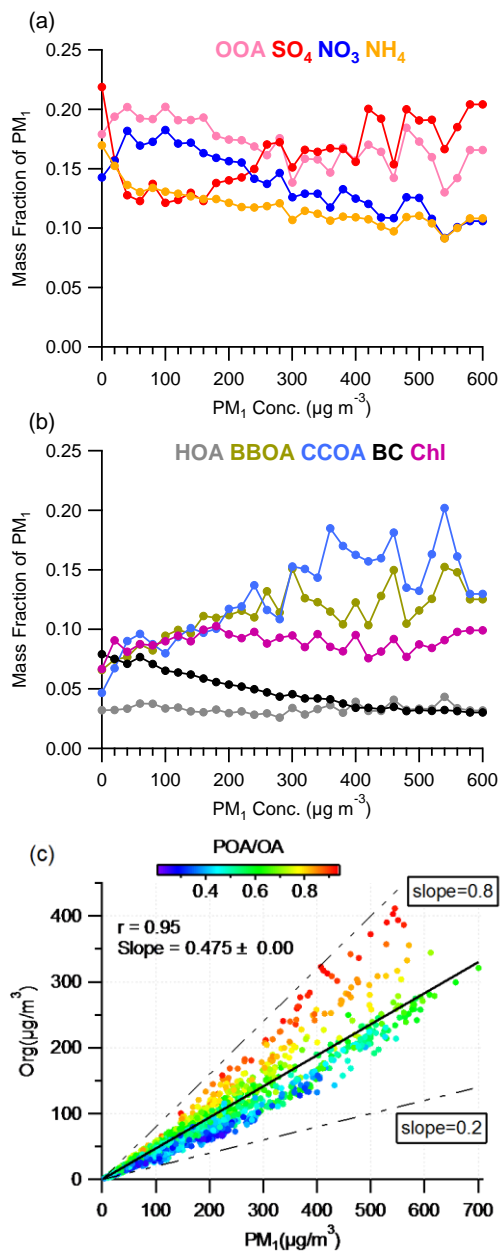
687

688

689

690

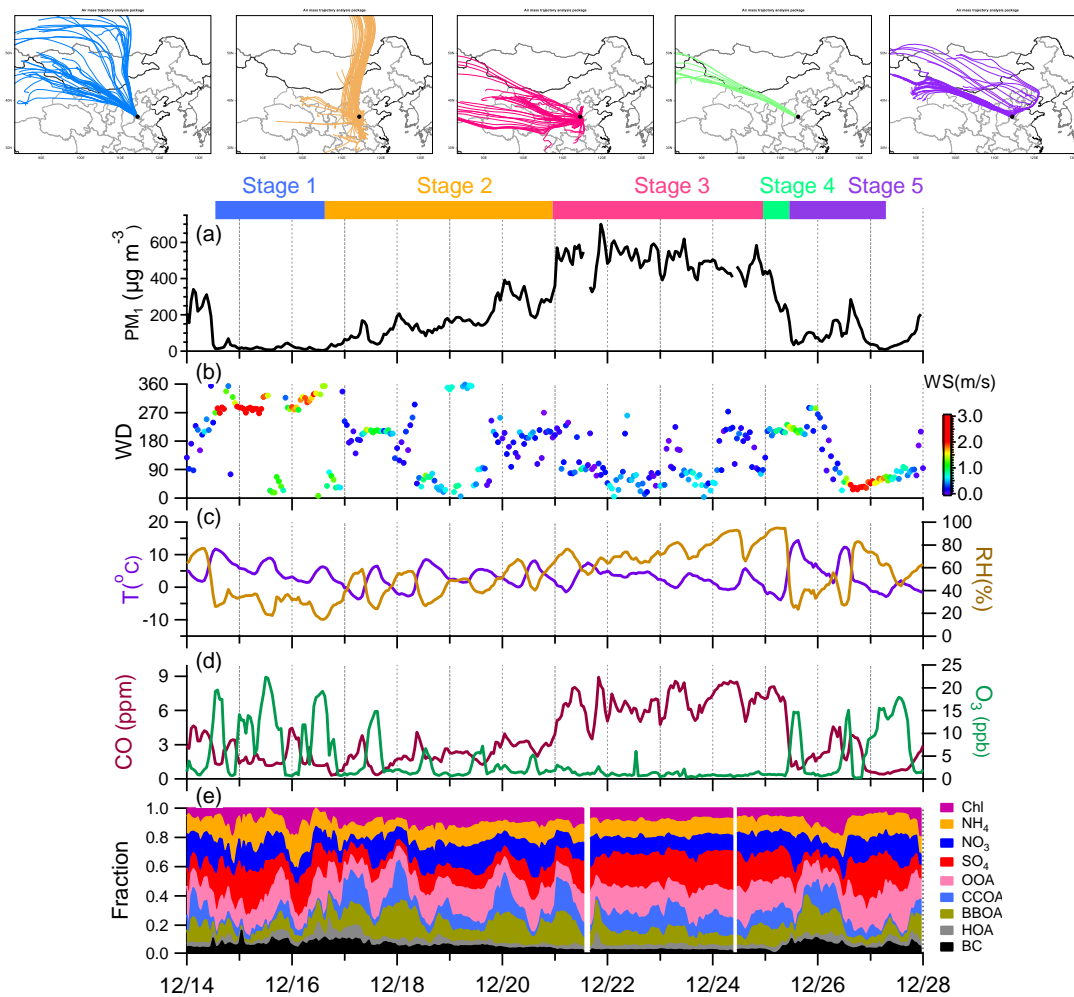
Figure 8. (a) Average PM_{10} composition and bivariate polar plots of PM_{10} concentration as a function of wind speed and wind direction for polluted and non-polluted periods. (b) Average concentration of PM components, gas phase species and average meteorological conditions during polluted and non-polluted days, with their polluted/non-polluted ratios shown in the top panel.



691

692 **Figure 9.** (a, b) Variations of the mass fractions of aerosol species as a function of PM₁ concentration. (c) Correlation plot of organics
 693 and PM₁ concentrations, colored by the mass fraction of POA in total OA.

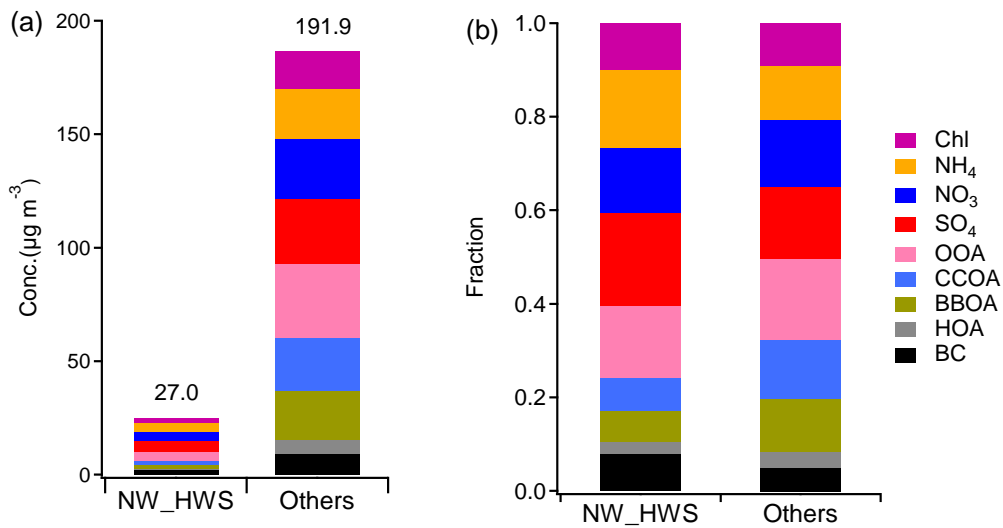
694



695

696 **Figure 10.** Evolution of (a) PM₁ concentration; (b) wind direction (WD) and wind speed (WS); (c) Temperature (T) and relative
 697 humidity (RH); (d) mixing ratios of CO and O₃; (e) mass fractions of aerosol species during a severe haze cycle from December 14 to
 698 December 28, 2016. The event was divided into five stages, with back trajectories of each stage shown on the top.

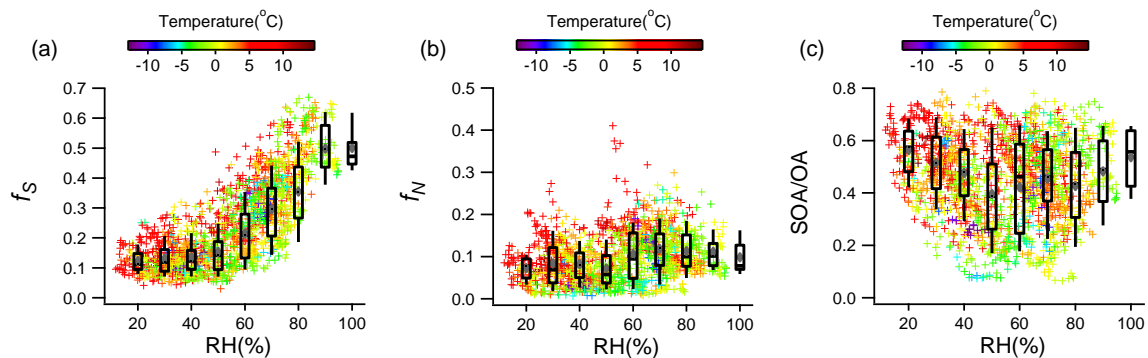
699



700

701 **Figure 11.** Comparisons of (a) mass concentrations of all PM₁ species and (b) fractional contributions of PM₁ species between
 702 “NW_HWS” and “Others” for the entire study period. The “NW_HWS” refers to high winds from the northwestern areas, and “Others”
 703 refers to the remaining.

704



705

706 **Figure 12.** Variations of (a) f_s , (b) f_N , and (c) the mass fraction of SOA in total OA plotted against increasing RH. The data are also
 707 binned according to RH values, and the mean (cross), median (horizontal line), 25th and 75th percentiles (lower and upper box), and 10th and
 708 90th percentiles (lower and upper whiskers) are shown for each bin.